J Geod (2011) 85:205–228
DOI 10.1007/s00190-010-0430-2

ORIGINAL ARTICLE

Lunar gravity field determination using SELENE same-beam differential VLBI tracking data

S. Goossens · K. Matsumoto · Q. Liu · F. Kikuchi · K. Sato · H. Hanada · Y. Ishihara · H. Noda · N. Kawano · N. Namiki · T. Iwata · F. G. Lemoine · D. D. Rowlands · Y. Harada · M. Chen

Received: 5 April 2010 / Accepted: 20 November 2010 / Published online: 7 December 2010

Abstract A lunar gravity field model up to degree and order 100 in spherical harmonics, named SGM100i, has been determined from SELENE and historical tracking data, with an emphasis on using same-beam S-band differential VLBI data obtained in the SELENE mission between January 2008 and February 2009. Orbit consistency throughout the entire mission period of SELENE as determined from orbit overlaps for the two sub-satellites of SELENE involved in the VLBI tracking improved consistently from several hundreds of metres to several tens of metres by including differential VLBI data. Through orbits that are better determined, the gravity field model is also improved by including these data. Orbit determination performance for the new model shows improvements over earlier 100th degree and order models, especially for edge-on orbits over the deep far side. Lunar Prospector orbit determination shows an improvement of orbit consistency from 1-day predictions for 2-day arcs of 6 m in a total sense, with most improvement in the along and cross-track directions. Data fit for the types and satellites involved is also improved. Formal errors for the lower degrees are smaller, and the new model also shows increased correlations with topography over the far side. The estimated value for the lunar GM for this model equals 4902.80080 ± 0.0009 km^3/s^2 (10 sigma). The lunar degree 2 potential Love number k_2 was also estimated, and has a value of 0.0255 ± 0.0016 (10 sigma as well).

Keywords Lunar gravity · Differential VLBI · Orbit determination · Gravity field determination

S. Goossens (✉) · K. Matsumoto · F. Kikuchi · K. Sato · H. Hanada · Y. Ishihara · H. Noda
RISE Project, National Astronomical Observatory of Japan, 2-12 Hoshigaoka, Mizusawa, Oshu, Iwate, 023-0861, Japan
e-mail: sander@miz.nao.ac.jp

Q. Liu · N. Kawano · Y. Harada · M. Chen
Shanghai Astronomical Observatory, Shanghai, China

N. Namiki
Planetary Exploration Research Center, Chiba Institute of Technology, Tsudanuma, Narashino, Chiba, Japan

T. Iwata
Japan Aerospace Exploration Agency, Yoshinodai, Sagamihara, Kanagawa, Japan

F. G. Lemoine · D. D. Rowlands
Planetary Geodynamics Laboratory, Solar System Exploration Division, NASA Goddard Space Flight Center, Greenbelt, MD, USA

1 Introduction

Until recently, lunar gravity field models were determined from either 2-way tracking (where the up- and downlink stations are the same) or 3-way tracking (where they are different) between stations on Earth and a satellite orbiting the Moon. Due to the 1:1 spin-orbit resonance of the Earth–Moon system, this leads to a gap in the tracking data when the satellite flies over the far side of the Moon. This gap in coverage severely hampers the determination of the global lunar gravity field, and the standard way of dealing with this is to impose additional constraints on the solution in the form of regularisation to smooth the solution and make the inverse problem stable [see Lemoine et al. (1997) and Konopliv et al. (2001) for examples of gravity field solutions, and Floberghagen (2002) for a thorough discussion of the lunar gravimetric inverse problem].

The Japanese SELENE mission (Kato et al. 2008) has filled in the tracking data gap by employing a tracking

technique called 4-way Doppler (Namiki et al. 1999). SELENE consisted of three satellites: a main orbiter in a polar, circular orbit at an average altitude of 100 km above lunar surface, and two sub-satellites in polar, elliptical orbits, called Rstar and Vstar. One of these sub-satellites, Rstar, carried communication instruments to forward a radio signal to the main orbiter, and to receive the return signal. By establishing this link while the main orbiter was over the far side of the Moon, the first tracking data over the far side were collected. This has resulted in new lunar gravity field models. Namiki et al. (2009) reported the first results, a 90th degree and order spherical harmonics expansion of the lunar gravitational potential based on data collected in the first 5 months of the SELENE mission. This model named SGM90d clearly resolves ring-shaped structures associated with basins on the far side. Matsumoto et al. (2010) reported an updated model, named SGM100h, a 100th degree and order spherical harmonics expansion based on all 4-way tracking data that were obtained. Owing to the tracking data over the far side, this model can estimate the coefficients up to degree and order 70 without application of an a priori constraint.

In addition to the 4-way tracking data, SELENE collected one more tracking data type not used extensively before in planetary gravity mapping: same-beam differential VLBI (Very Long Baseline Interferometry) tracking between the two sub-satellites, and two stations on Earth. VLBI tracking is based on the delay between the arrival times of a radio source at two different stations constituting a baseline, and as such, it carries information on the angular position of the source (e.g. Thornton and Border 2000). Since 2-way (Doppler or range) tracking has only sensitivity in the line-of-sight direction from the station to the satellite, including VLBI data improves the three-dimensional positioning of the satellite. The accuracy of VLBI tracking is limited by, amongst others, delay measurement accuracy, media effects and clock offset errors. These errors can be largely removed in differential measurements, where delay differences from two sources close to each other in the sky are measured. As a result of the differencing, clock errors and instrumental errors are cancelled, and if the propagation paths of both sources are nearly identical, most media effects are removed as well (Thornton and Border 2000). The benefits of using differential VLBI were recognised early on (Counselman III et al. 1972, 1973; Counselman III 1973), followed by a wide range of successful applications. To list a few, differential VLBI has been used to determine the relative position of the Apollo 16 and 17 lunar rovers (Salzberg 1973), to determine the lunar librations (King et al. 1976), to derive winds on Venus from the Pioneer probes (Counselman III et al. 1979) and from the VEGA balloons (Sagdeev et al. 1986; Preston et al. 1986) and to observe the descent of the Huygens probe on Titan (Witasse et al. 2006). Differential VLBI has furthermore been used in orbit determination of planetary satellites (Border et al. 1992; Folkner et al. 1993), and VLBI tracking of spacecraft contributes systematically to planetary ephemeris solutions (e.g. Folkner et al. 2009).

The same-beam differential VLBI measurements on SELENE have the goal to improve the orbit estimates of the sub-satellites and to improve the estimate of especially the lower degrees of the spherical harmonic expansion of the lunar gravitational potential (Heki et al. 1999; Matsumoto et al. 2008). S and X-band signals broadcast from artificial radio sources on board both satellites are captured simultaneously at a station on Earth (hence they are called same-beam observations), by tracking the midpoint of the satellites in the sky seen from the Earth. The differences of delay between arrival times of the signal at different stations, further differenced between the two satellites, constitute a doubly differenced 1-way range, where most of the media effects and clock errors on the data are cancelled through the differencing. The system used in SELENE is further described in Hanada et al. (2008) and in Hanada et al. (2010). Analysis of the actual VLBI data collected from SELENE has shown that a picosecond accuracy (equivalent to a 0.3 mm differential VLBI residual) is possible with these data (Kikuchi et al. 2009), and that media delays were indeed kept to a minimum (Liu et al. 2010a).

The orbit determination software used to process the tracking data into satellite orbits is GEODYN II (Pavlis et al. 2006). The same-beam differential VLBI data are modelled in this software as follows, with $S_i \rightarrow T_i$ denoting a link from satellite i to station i ($i = 1, 2$ in both cases):

$$[(S_1 \rightarrow T_1) - (S_2 \rightarrow T_1)] - [(S_1 \rightarrow T_2) - (S_2 \rightarrow T_2)] \quad (1)$$

It should be stressed that the differences in this equation are different from those used in GPS double-difference modelling (e.g., Seeber 2003). Light times are computed so that ranges from the same satellite to different stations have the same transmit epoch, instead of using the same receiving epoch at different stations. These differences are further denoted in this paper by singly-differenced VLBI measurements.

The research presented here is the result of the analysis of data of an extensive VLBI tracking campaign, lasting 14 months. All same-beam differential VLBI have been correlated and used for the purpose of orbit and gravity field determination. The results presented here show how these tracking data help to improve the orbit estimates of the sub-satellites, and consequentially, how the data help to improve the estimate of the lunar gravity field model.

This paper is structured as follows: Section 2 describes the VLBI data. In Sect. 3, results for orbit determination using these data are presented. Based on these results the lunar

gravity field is determined, which is described in Sect. 4. Discussion of the results can be found in Sect. 5, and the paper ends with conclusions and an outlook in Sect. 6.

2 Brief description of VLBI tracking data

This section briefly describes the VLBI tracking components (satellites and station-network), and characteristics of the VLBI data used.

2.1 Satellites and network-stations

SELENE consisted of three orbiters: a main orbiter in a polar, circular orbit at an average altitude of 100 km above lunar surface in its nominal mission (which lasted from October 2007 until October 31, 2008) and two sub-satellites in polar elliptical orbits of initially 129 by 792 km (called Vstar) and 120 by 2395 km (called Rstar), respectively. The satellites were launched on September 14, 2007, from Tanegashima Space Center. The sub-satellites were released in their orbits on October 9, 2007 (Rstar) and October 12, 2007 (Vstar). The main orbiter was three-axis stabilised whereas the sub-satellites were spin-stabilised satellites (so-called "free-fliers", as their orbit was not maintained by correction manoeuvres). The sub-satellites have an octagonal prism body, with the side-panels covered by solar cells. S/X-band dipole antennas are placed on top of the satellites, and they are aligned with the spin-axis. The satellites measure 1 m by 1 m by 0.65 m and their total mass is about 45 kg. The spin-rate of the spacecraft was determined from high-rate (10 Hz) Doppler data, and it was found to be 0.1833 Hz for Rstar (a spin period of 5.46 s) and 0.1875 Hz for Vstar (a spin period of 5.33 s) (Liu et al. 2010b). This spin induces a bias on the Doppler data, in this case of about 1 mm/s, and this small value comes from computing the bias due to the changing polarisation of the signal and the remaining frequency difference due to the turn-around ratio at the spacecraft (see Konopliv et al. (2001) for results concerning Lunar Prospector, also a spin-stabilised satellite). This bias was estimated (see below) and it was found to be around the predicted value.

The sub-satellite Rstar served as the relay satellite for the 4-way Doppler data, and both sub-satellites were used in the same-beam VLBI tracking campaign. During the entire mission, standard 2-way data (range and Doppler) were collected from all three satellites, in addition to the 4-way data, whenever there was a chance (Matsumoto et al. 2008; Matsumoto et al. 2010). There were no 3-way Doppler data obtained.

The VLBI tracking campaign used the Japanese VERA (VLBI Exploration of Radio Astronomy) network, which consists of four stations, located in Iriki, Ishigaki, Mizusawa and Ogasawara (Kobayashi et al. 2003). There were also two international tracking campaigns, each of about 1 month duration, during which stations in China, Germany and Tasmania participated. For future reference, the coordinates of all participating tracking sites are listed in Table 1. The inclusion of the overseas stations means that longer baselines than can be achieved with the VERA stations only can be used, and this means a better sensitivity to the motion of the spacecraft, and should thus lead to a more precise orbit. VLBI data were collected in tracking sessions of an average of 8 h per day, 3 times a week for the VERA stations (Hanada et al. 2008), complemented by the aforementioned intense, 1-month international tracking sessions.

Due to its natural orbital evolution, Rstar crashed into the Moon on February 12, 2009, ending the collection of both 4-way data and same-beam VLBI data between the sub-satellites. The main orbiter ended its lifetime with a controlled crash on the Moon on June 10, 2009, and tracking for Vstar was stopped on June 29, 2009. The altitude history of both sub-satellites spanning the VLBI data period is given in Fig. 1, in the form of perilune and apolune altitudes above lunar surface. The eccentricity change for Rstar (and its ultimate lunar impact) is due mostly to the third-body gravitational perturbation of the Earth. The orbit for

Table 1 Earth-fixed coordinates and antenna diameters for the Japanese VERA stations and the overseas stations (i.e. not in Japan, country listed) used in the VLBI tracking of SELENE

Station name	Antenna diameter (m)	Earth-fixed coordinates (km)		
		X	*Y*	*Z*
Iriki (VERA)	20	−3521.71958	4132.17467	3336.99422
Ishigaki (VERA)	20	−3263.99472	4808.05629	2619.94922
Mizusawa (VERA)	20	−3857.24182	3108.78481	4003.90054
Mizusawa[a]	10	−3857.23610	3108.80321	4003.88308
Ogasawara (VERA)	20	−4491.06881	3481.54479	2887.39957
Hobart (Tasmania)	26	−3950.23674	2522.34756	−4311.56254
Urumqi (China)	25	228.31072	4631.92279	4367.06397
Shanghai (China)	25	−2831.68691	4675.73366	3275.32769
Wettzell (Germany)	20	4075.53988	931.73526	4801.62937

The coordinates refer to the ITRF2000 system, epoch Jan 1, 2006

[a] In a few instances, when the Mizusawa 20 m antenna was under maintenance, the Mizusawa 10 m antenna was used instead

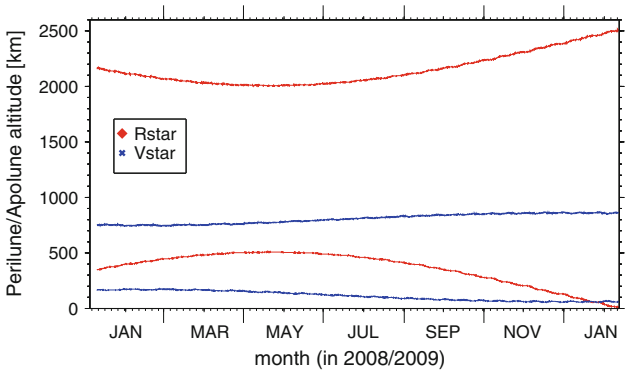

Fig. 1 Perilune and apolune altitudes above lunar surface for both Rstar and Vstar, during the VLBI data campaign

Vstar is much more stable. More detailed descriptions of the SELENE satellites, orbits and 2-way and 4-way tracking data can be found in Matsumoto et al. (2010).

2.2 VLBI data characteristics

The strength of the differential same-beam VLBI data derives from the differencing out of common measurement errors, resulting in a precise observation, but if the differential measurement is performed using a carrier channel with a single-frequency, then the total phase delay is ambiguous as the phase delay can only be determined up to a fraction of a cycle (e.g., Border et al. 1992; Thornton and Border 2000). To overcome the cycle ambiguity, and increase the accuracy of the measurement, a multi-frequency method was used, with three carriers in S-band (2,212, 2,218 and 2,287 MHz) and one in X-band (8456 MHz). Still, severe conditions on the data must be met in order to determine the cycle ambiguity, regarding the phase noise, a priori delay, and ionospheric influences (Kono et al. 2003). Pre-mission analysis and tests showed that the same-beam VLBI measurements as implemented for SELENE should be able to meet these conditions (Liu et al. 2007; Kikuchi et al. 2008).

Over the course of 14 months, starting in January 2008 with the full observations according to schedule (there were test observations prior to this period), same-beam and switching VLBI data were collected. As opposed to same-beam VLBI (which are taken when the separation angle between the spacecraft is smaller than the beamwidth), switching VLBI consists of tracking Rstar and Vstar consecutively, switching back and forth between the two spacecraft. In this way, most of the media delays can be cancelled as well although fluctuations with periods shorter than the switching period (typically in the order of a few minutes) remain. The results presented in this work, however, do not contain the switching VLBI data, as their correlation was not finished at the time of this analysis. Initial tests of the data showed that the differential phase delay of the X-band signal can be estimated within an error of below 1 ps (0.3 mm) (Kikuchi et al. 2009). Due to the narrow beamwidth of the X-band data, there were only few opportunities for collection of these data. S-band data are available in larger quantities because of the wider beamwidth, and further analysis of these data showed that the cycle ambiguity could be determined for a large portion of the data (roughly 85%), resulting in a differential phase delay with an error of a few picoseconds (roughly 1 mm) for small separation angles of the spacecraft, and about 10 ps (3 mm) for larger separations (Liu et al. 2010a). These accuracies include considerations of the effects of the ionosphere and atmosphere. In Liu et al. (2010a) it is shown that the combined (atmospheric, ionospheric and instrument) short-term effects are between 1 and 2.5 mm for small and larger separation angles between the satellites. Long-term ionospheric effects can be cancelled if S-band and X-band data are taken simultaneously, but in the case of S-band data only, corrections using GPS-data need to be applied. Liu et al. (2010a) also showed that the long-term ionospheric effects were mostly cancelled in the same-beam observations. In the period of SELENE observations, the sunspot number was also relatively low. Considering long-term atmospheric effects, their effect was shown to be reduced to several cm through same-beam observations. Remaining long-term effects will be dealt with by estimating a bias on the data, see also further on in Sect. 3.

All the same-beam S-band data have been correlated, resulting in roughly 430 h distributed over 192 days between January 2008 and February 2009 (estimated from counting the data points for one representative baseline for each observation day). The data were processed in 60 s integration intervals during correlation. This resulted in 142,586 data points to be used in orbit and gravity field determination. For contributions to orbit and gravity field determination, this is to be compared with 78,004 4-way data points, and several million 2-way Doppler data points, amongst which about 160,000 were for Rstar and 43,000 for Vstar (Matsumoto et al. 2010). Geographical coverage of the VLBI data is given in Fig. 2.

3 Orbit determination for the sub-satellites with VLBI data

Initial orbit determination tests of orbit overlap analysis for Rstar and Vstar have shown the improvements that can be achieved by including same-beam differential VLBI data: from a few hundreds of metres when using Doppler/range data only, to a 10-m level when including the SELENE VLBI data, and a few metres better when the overseas stations (constituting longer baselines) are included (from results presented in (Kikuchi et al. 2009) and (Liu et al. 2010a), using isolated test cases with arcs of less than 3 days long). In this work, the full set of same-beam S-band differential VLBI

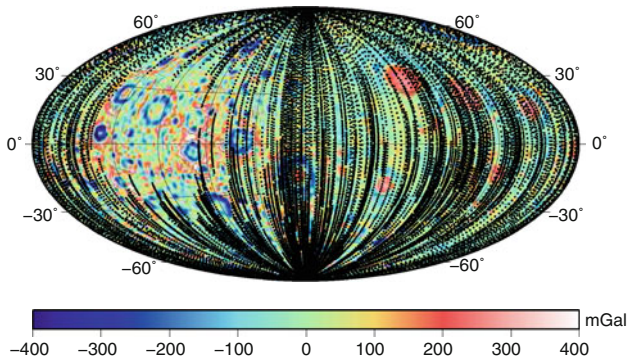

Fig. 2 Geographical VLBI data coverage, using the location of Rstar, plotted on *top* of gravity anomalies for the SGM100h model evaluated at the lunar surface in a spherical approximation. The *anomalies* are plotted in a Hammer projection centred on 270° eastern longitude, with the near side on the *right-hand side* and the far side on the *left-hand side*

data (hereafter simply called VLBI data) will be used consistently over the span of the entire SELENE mission, thus marking the first extensive and consistent use of such data. This section deals with the results from orbit determination, which will form the basis of using the VLBI data in lunar gravity field determination, described in the next section. First the data processing strategy and orbit determination parametrization will be described, followed by discussion of results concerning data fit and short-term orbit predictions. Results are summarised at the end of this section.

3.1 Data processing and orbit parametrization

The tracking data are processed with the GEODYN II software. The version of GEODYN II used here has been specifically modified to include interplanetary 4-way Doppler data and the interplanetary singly differenced VLBI data as described in the introduction. Tracking data are divided into arcs, which are continuous spans of time during which the orbit is integrated and over which parameters are estimated. As always in the dynamical approach taken here, arc length is limited due to the build-up of errors that occur when long time spans are integrated. These errors build up because of imperfect force modelling, and imperfect knowledge of for example the state vector at epoch, and other parameters that influence the orbit integration. If the errors grow too large, the assumption of linearity on which the least-squares orbit estimation procedure is based does not hold.

Previous lunar gravity field solutions using SELENE data, but without the VLBI data, were based on arc lengths for Rstar of on average 12 h (supporting online materials Namiki et al. 2009) or 2.6 days (Matsumoto et al. 2010), and arcs for Vstar of on average 2.4 days. Arc lengths were decided by trading off sensitivity with respect to gravitational parameters versus the aforementioned build-up of errors. This was also largely driven by tracking data coverage in time. Rstar and Vstar 2-way tracking data were obtained through the 64m antenna of Usuda Deep Space Center (UDSC). Due to restrictions on the usage of UDSC, and its involvement in 4-way tracking, there was a limitation on the 2-way tracking intervals to Rstar and Vstar (Matsumoto et al. 2010), leaving only short passes for Rstar and Vstar. On average, passes were 32 and 24 min long per day for Rstar and Vstar, respectively, usually separated by at least 1 day. For comparison, the orbital periods of Rstar and Vstar were roughly 4 and 2.5 h, respectively. Figure 3 shows the time-wise data coverage for 1 week in April, 2008. During 4-way tracking Rstar was also tracked with 2-way data, which led to increased tracking for Rstar, with several passes close together. Through including the precise VLBI data (as well as through simply including more data), the expectation is that longer arc lengths can be used, thus increasing the sensitivity to especially the lower degrees of the spherical harmonics expansion of the lunar gravitational potential (e.g., Matsumoto et al. 2008). The aim here is to use nominal arc lengths of 1 week for both Rstar and Vstar. The influence of arc length on the orbit and gravity results is discussed in Sect. 5 as well.

Estimated parameters are, as usual, divided into arc (or local) and common (or global) parameters, where the first are parameters valid only for a particular arc (e.g. the state vector at epoch, bias parameters on the data, etc.), and the latter

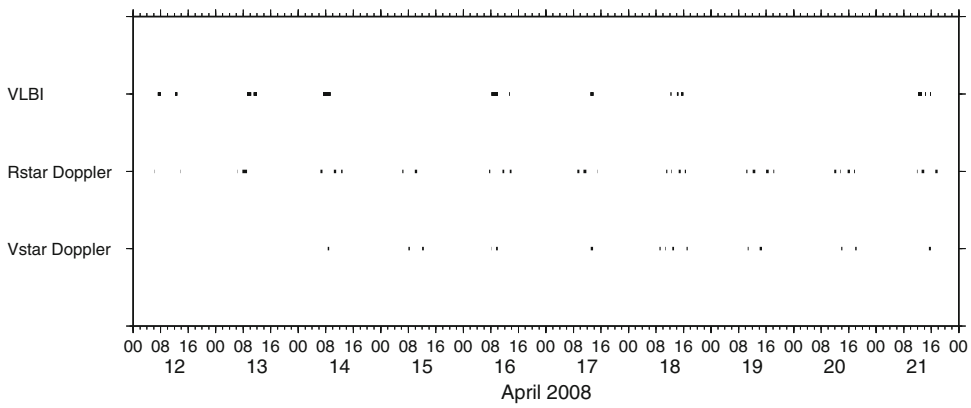

Fig. 3 Time-wise data coverage showing periods for which there was Rstar and Vstar Doppler and VLBI data, for 1 week in April 2008. Time coordinates are in Universal Time. Range data are left out since they were always collected together with Doppler data

are parameters common to all arcs (such as the gravity field coefficients), respectively. As the current focus is on assessing the precision of orbit determination, initially no global parameters are estimated. Instead, this is deferred to the next section. Estimated arc parameters per satellite are the state vector at epoch, one scaling coefficient C_R for solar radiation pressure per arc, biases per pass on both the 2-way range data (because of ambiguities and unmodelled media effects) and Doppler data (induced by the spin of the spacecraft), and one set of empirical accelerations in along-track (in the flight-direction) and cross-track (normal to the orbital plane) directions with a once-per-orbital-revolution signature (i.e. sine and cosine coefficients). The C_R coefficient and empirical accelerations are mainly meant to absorb mismodelling of non-conservative forces (solar radiation pressure). A priori uncertainties for C_R were 10 % (0.1 at a nominal value of 1.0), and those for the empirical accelerations were set high at 10^{-5} m/s^2 so that they can adjust almost freely. More about the influence of these parameters on the orbit determination will be mentioned in the results section.

When the VLBI data are included in the orbit determination, biases per pass per baseline are also estimated. These biases are meant to absorb ambiguity cycles on the data that slipped through in the correlation processing, and, to a smaller extent, to absorb remaining media effects (as mentioned they are small, but they can be present nevertheless). In principle the correlation process will indicate whether or not the cycle ambiguity was determined, but since the data are processed in batches of 30 min, there is the possibility that there is an ambiguity cycle jump between consecutive batches, or on the whole pass (Liu et al. 2010a). Inspection of estimated biases after orbit determination will thus show whether this was the case (see also Sect. 3.2.5).

The VLBI data are derived from the differences in delays between two different satellites and stations, and this means that when the VLBI data are used in orbit determination, the orbits of Rstar and Vstar are determined simultaneously. Their orbits are thus integrated at the same time, making use of the same global parameters and force models (though with satellite-dependent arc parameters, of course), assuring consistency. Orbit determination with VLBI data is performed by applying a full-scale force modelling, together with precision measurement modelling. In addition to using the VLBI data, the 2-way Doppler and range data for Rstar and Vstar are also included. The SELENE 4-way data were also collected through Rstar, but since they contain a link to the main satellite, they are left out of the orbit determination for the sub-satellites described here. They will of course be included in the gravity field determination described in the next section.

As reference gravity field, the SGM100h model (Matsumoto et al. 2010) was used. Although this model was derived by including 2-way tracking data from the sub-satellites, it did not include the VLBI data, so they are independent with respect to this model. The DE421 lunar ephemeris and librations solution (Williams et al. 2008; Folkner et al. 2009) was used to obtain the planetary positions when computing third-body perturbations from the planets, and these ephemeris were also used to define the lunar coordinate system. The tidal force of the Earth and Sun that affects the lunar gravity field was modelled with a potential degree 2 Love number $k_2 = 0.024$, which is the value derived with the SGM100h model. Solar radiation pressure was modelled using a cannonball model, where the cross-sectional area of the satellite is constant, scaled by a coefficient C_R. Displacements on Earth stations due to solid Earth tides, pole tide loading and ocean tides per site are included as well. Measurement corrections coming from media and relativity effects are included in the processing software.

3.2 Orbit determination results

Orbit determination for Rstar and Vstar was performed as described above. Results are assessed in different ways: by inspecting post-fit data residual levels, and by inspecting results for orbit predictions. In addition, the effects of changing data weights and the effects of solar radiation pressure are discussed, as well as the values and meaning of the estimated biases on the VLBI data.

3.2.1 Post-fit data residuals

Figure 4 shows the RMS of fit per arc of the 2-way Doppler data for both satellites. In order to assess the impact of the VLBI data, orbit determination with and without these data was performed. Data weights used in the orbit determination were chosen to be 1 mm/s for 2-way Doppler data, 2 m for range data and 1 cm for same-beam VLBI data. Figure 4 shows that the data fit for Rstar is well below the level of the data weight: in general, a level of fit of 0.2 mm/s is achieved. For Vstar the level of fit is worse when compared with Rstar, at 0.4 mm/s, but overall this is also well below the chosen data weight. Results for Vstar show more variations when compared with Rstar. This is mostly due to having less tracking data, as can also be inferred from the example shown in Fig. 3. For Rstar, towards the end of the mission, data fit levels go up as Rstar's perilune altitude decreased, see also Fig. 1. This is also the case for Doppler residuals for Vstar when including VLBI data, since these data tie the two satellites together. Results for Doppler residuals when also including VLBI data are higher for both satellites. This is the effect of weighted least-squares, where changes in data weights for one measurement type affect the fit of the others. Range data are also included in the orbit determination process but their data fit is not shown here. The pattern of fit levels for them is similar to that of the Doppler data, with on average a level

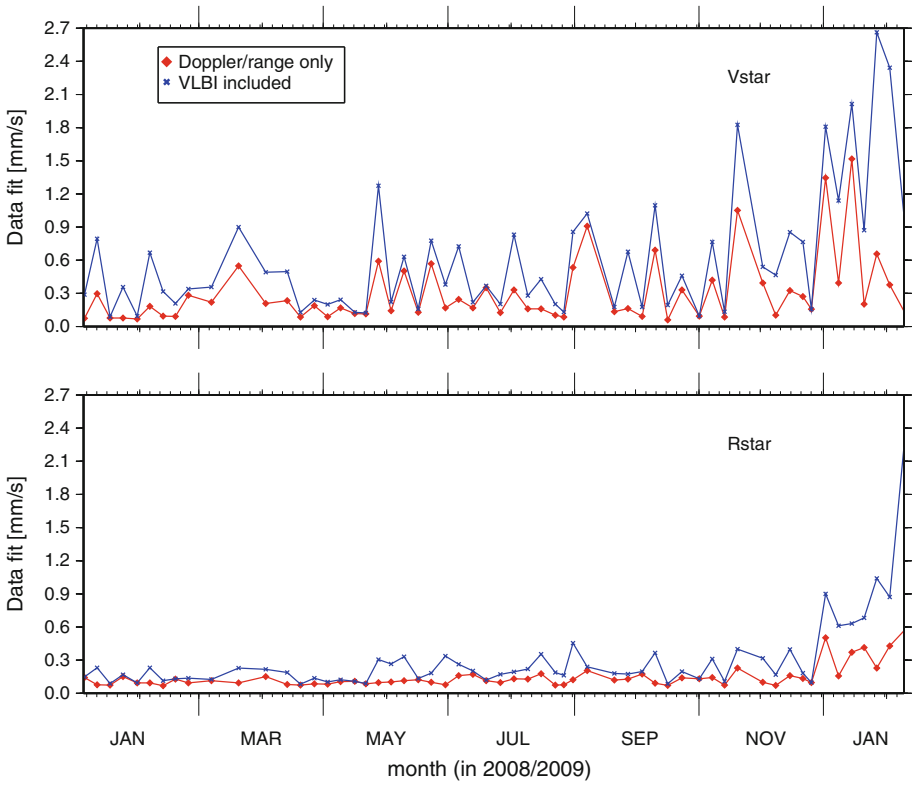

Fig. 4 The RMS of Doppler data residuals for both Rstar (*bottom*) and Vstar (*top*), during the entire SELENE mission. The *labels* are the same for both plots, so the legend is displayed just once

of fit of 1 m for both Rstar and Vstar, deteriorating slightly when VLBI data are included.

The RMS of fit for the VLBI data are shown in Fig. 5. With a data weight of 1 cm, the actual RMS of fit is quite close to this level. Since the data were shown to have an even lower intrinsic noise level (Kikuchi et al. 2009; Liu et al. 2010a), a data weight of 1 mm was also used. This indeed brings the level of fit of the VLBI data down as can be seen from the Figure, but it never gets down to the 1-mm data weight level. Towards the end of lifetime of Rstar the VLBI data fit levels increase, as also for the Rstar Doppler residuals. The value of 1 mm might be too strict in terms of remaining atmospheric and ionospheric effects, which are thought to be several cm and several mm, respectively (Liu et al. 2010a). In the case of atmospheric effects, the larger part of the long-term effects are either modelled within the software or absorbed by the estimated biases, as the RMS of the VLBI data residuals is in general smaller than 1 cm.

For further inspection of the VLBI residuals, an example of residuals during one arc is shown in Fig. 6. Residuals per baseline are indicated with the names of the stations. Both plots that are shown are from one and the same arc, showing residuals mostly within the ± 1 cm level, but upon inspection they show different behaviour. In the bottom plot, showing residuals during a relatively long pass, they are mostly scattered around zero without systematic signals, as normally expected. The top plot, however, also for a relatively long pass, does show systematic behaviour, especially for the Ishigaki–Mizusawa and Ishigaki–Iriki baselines. These baselines show a sinusoidal form of the residuals, indicating a residual systematic signal in them. This was found for several instances during the whole mission period, mostly when passes were long, though not always, as the bottom plot indicates. It should again be stressed that both residual passes are within one and the same arc, meaning it is unlikely to be a systematical error in the processing, since then a similar signal should have been visible in the bottom plot as well. One reason for the remaining signal could be effects of solar radiation pressure mismodelling, but shorter arcs (where presumably the error in solar radiation pressure mismodelling is smaller) produce the same results. Only shortening the arc to the duration of the pass makes the signal disappear, which means it is likely absorbed by a state-vector adjustment, which strengthens the suspicions that it is a remaining dynamical signal.

The sinusoidal signal has a period of slightly over 1.5 h, which is roughly equal to the synodic period between Rstar's and Vstar's orbit (using $P_r = 4$ h for Rstar and $P_v = 2.5$ h for Vstar, one finds using $1/P_s = 1/P_r + 1/P_v$ that $P_s = 1.53$ h). This could perhaps be an indication that for certain geometries, the orbits of Rstar and Vstar cannot be untangled using the VLBI data (as they are in principle a data type using the orbit differences between the two satellites), or that at least some residual orbital signal remains. Anticipating the

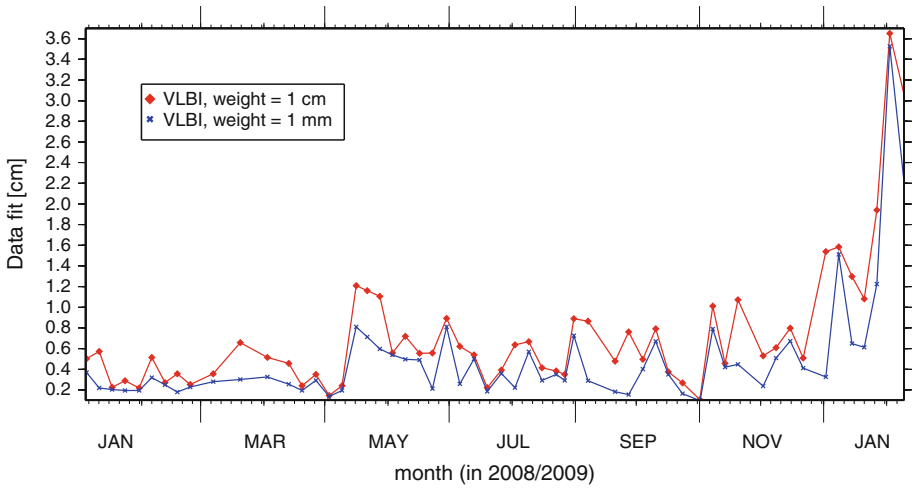

Fig. 5 The RMS of VLBI data residuals during the entire SELENE mission. Results for different data weights for the VLBI data in the orbit determination process are shown

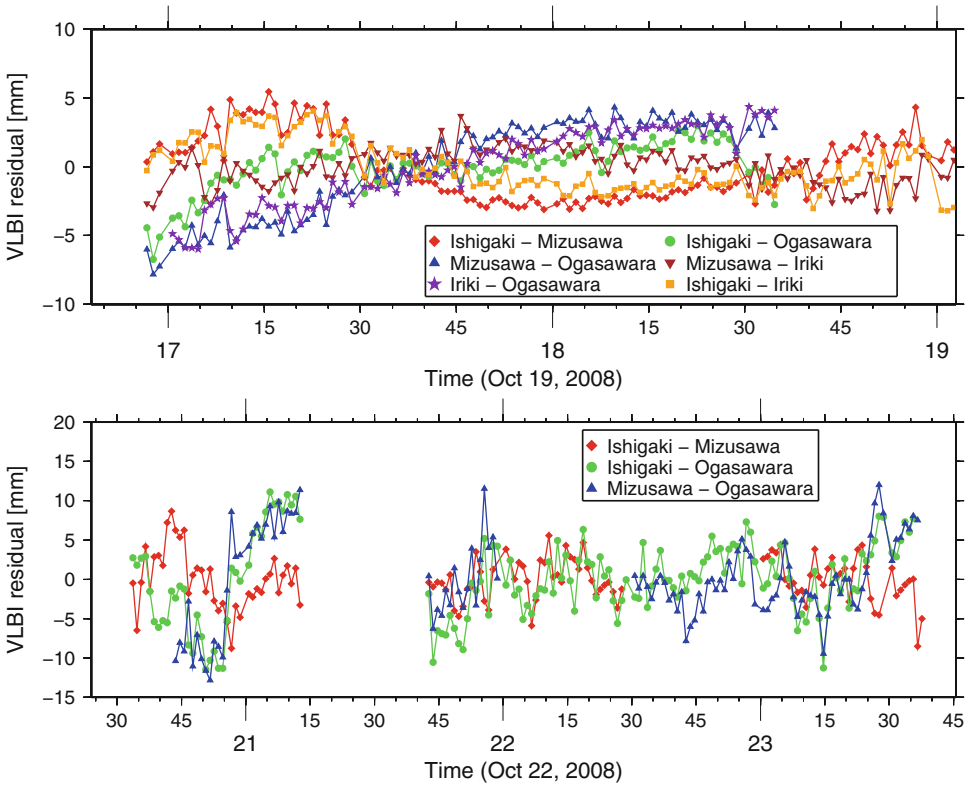

Fig. 6 VLBI residuals plotted as a time series for two passes during one arc. Residuals are plotted separately per baseline, with baselines indicated by the station names. Times indicated are hours and minutes (UT)

gravity analysis that will be discussed in the next section, it can already be stated here that the signal did not disappear when this arc was reprocessed with a gravity field model that was derived using this arc and these data, indicating that it is not directly related to a gravity feature.

3.2.2 Orbit precision assessment through overlaps

In order to establish some level of precision for the orbits, orbit differences during overlaps are investigated. These orbit differences are computed by propagating an estimated orbit beyond its time span of tracking data used, forming an overlap with a consecutive arc. Orbit differences during the overlapping part are then computed, and these predictions indicate consistency of the computed orbits. From the 1 week arcs, 24 h predictions are chosen in order to ensure multiple orbital revolutions of both satellites. Orbit prediction tests with 48 h overlaps did not change the results. Results for both Rstar and Vstar are shown in Fig. 7.

It is immediately striking how much the VLBI data contribute to improving the orbit consistency: results for both Rstar and Vstar with Doppler and range data only are at the 100-metre level, whereas including VLBI data brings the orbit differences down to several tens of metres or less.

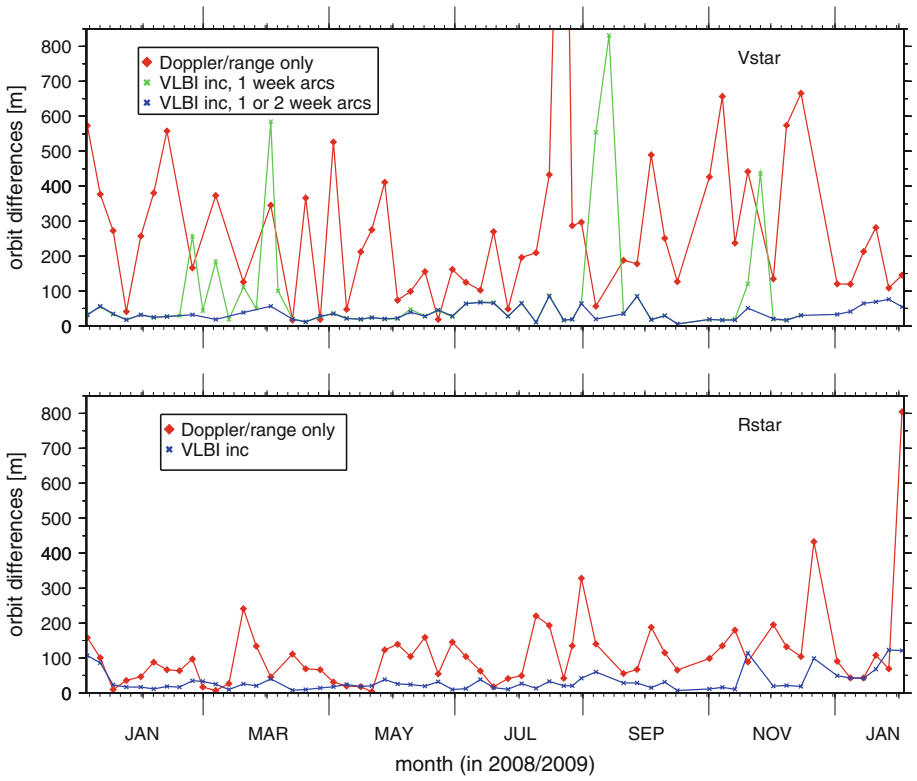

Fig. 7 RMS of orbit differences for 24 h predictions per arc and per sub-satellite during the entire SELENE mission period. The value on the *vertical-axis* is the root-sum-square value over all three directions, representing a total three-dimensional orbit overlap value. Results for Doppler/range data only, and VLBI data included in the orbit determination process are shown

This is similar to what has been reported before on short (a few days), isolated test arcs (Kikuchi et al. 2009; Liu et al. 2010a), except here the results are consistent for the entire SELENE mission, for longer arcs. It is also striking that while the orbit differences for Rstar and Vstar are different when using Doppler and range data only, they become more consistent with each other when the VLBI data are included. This is because these data tie the orbits together.

The contribution of the international campaigns (that lasted roughly from January 12–20 and May 22–July 02, 2008) was investigated by computing overlaps with and without these data. The effect of the campaigns is small (which is why Fig. 7 does not include these results): in general the orbits get a few metres better with the foreign stations, as was also shown in Liu et al. (2010a) for an isolated test case. In the January period the effect is even reversed, with better orbits without the foreign stations. This can point to either different intrinsic accuracies due to different antenna characteristics, or increased atmospheric and other effects for the longer baselines. But overall, the biggest improvement in orbit consistency comes from simply including the VLBI data. The foreign campaigns did increase the data amount and length of the baselines, but they did not fill in gaps in tracking in time.

The results for the orbit differences are detailed further in Table 2, which shows the average RMS of orbit differences in the three separate directions in the local satellite frame, radial, along and cross track, as well as the average of the total RMS shown in Fig. 7. Results discussed further on from Fig. 8 are also included. The results for the separate directions indicate where the strength of the VLBI data lies: in improving especially the orbit consistency in along and cross track direction. This is expected because the VLBI data have a plane-of-sky sensitivity. Results for Rstar show a small deterioration in radial direction when compared with the Doppler and range only results, but this deterioration is overshadowed by the drastic improvements in the other directions.

Table 2 Average values for the RMS of orbit differences as shown in Fig.7, separated per direction in the local satellite orbit frame

Data	VLBI weight	Orbit differences (m)			
		Radial	Along	Cross	Total
Results for Rstar					
DR	–	5.72	88.30	61.46	112.83
DRV	1 cm	6.66	28.65	12.26	33.09
DRV	1 mm	11.91	40.17	13.37	45.20
DRV	20 cm	5.76	53.12	28.72	63.11
Results for Vstar					
DR	–	13.00	233.97	130.83	288.28
DRV	1 cm	7.15	31.00	13.05	36.08
DRV	1 mm	9.42	43.42	16.29	49.63
DRV	20 cm	7.15	55.62	33.57	68.9

Results shown later on in Fig. 8 are also included
DR stands for using Doppler and range data
DRV stands for using Doppler, range and VLBI data

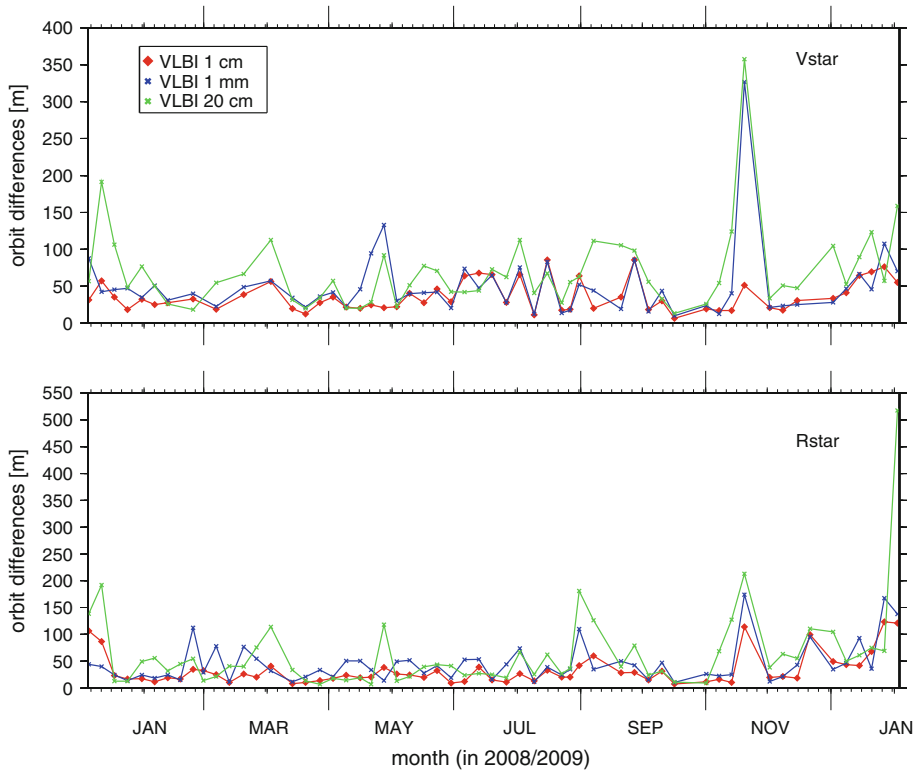

Fig. 8 RMS of orbit differences for 24 h predictions per arc and per sub-satellite using different data weights for the VLBI data. The value on the *vertical-axis* is again the root-sum-square value over all three directions

The plots for Vstar using VLBI data in Fig. 7 have one more additional result: using arc lengths of nominally 1 week, it was found that certain arcs resulted in large orbit differences, sometimes larger than when using Doppler data only. For some arcs, this was for example because there were few VLBI data. When comparing these results with orbit differences using arc lengths of 2 weeks (not shown here), it was found that for these outliers, 2 week arcs actually performed better, though on the whole they did not. So for those few periods, arcs for Vstar were extended to 2 weeks, while arcs for Rstar were kept the same.

The level of orbit differences for the sub-satellites using Doppler and range data only is quite large, considering that low-lunar orbiters typically have a precision at a level of 50–100 m, from Lunar Prospector orbit determination results (e.g., Carranza et al. 1999; Goossens and Matsumoto 2007) and from performance of SGM100h (Matsumoto et al. 2010). The difference with Lunar Prospector here is twofold: first, the amount of tracking data, and the ellipticity of the orbits of the sub-satellites. Lunar Prospector had continuous tracking, as opposed to the sub-satellites of SELENE, cf. Fig. 3. Orbit prediction results in Fig. 7 thus show how sparse tracking affects the orbit precision. This also explains the differences between results for Vstar and Rstar when using Doppler and range data only, as for Vstar the tracking was sparser than that for Rstar. Improvements from using VLBI data thus stem not only from using precise data, but also from simply using more data. And second, elliptical orbits have an inherently larger uncertainty for the determined state: covariance tests with the same amount of data for an elliptical and circular orbiter showed a larger a posteriori state vector uncertainty (a factor of about two in the test case considered) for the elliptical orbit.

3.2.3 Solar radiation pressure modelling

The use of VLBI data allows the increase of arc length. For longer arcs, however, non-conservative forces such as solar radiation pressure start to become significant, and it could very well be that mismodelling in that force is contributing to the orbit errors of Rstar and Vstar. To assess this, solar radiation pressure has been modelled in different ways. The standard way is to use a cannonball model, where the cross-sectional area of the satellite is constant. Solar radiation pressure is then scaled with a coefficient, C_R, as mentioned in Sect. 3.1. This approach has been taken here, and one C_R per arc per satellite is estimated. Additionally, one set of empirical accelerations in along and cross track direction per arc per satellite, with a once-per-orbital-revolution signature is also estimated. If these accelerations are not included, the orbit differences as shown in Fig. 7 are much larger, even when including VLBI data. Inspection of the estimated C_R values shows that the results for Rstar are relatively stable, with a value close to 1.0 most of the time, but values for Vstar show

a lot of variation. This can be due to having less Doppler data than Rstar. Inspection of the values of the estimated empirical accelerations also show a difference between Rstar and Vstar: for Rstar values are at about 10% of the solar radiation pressure induced accelerations, whereas they are 50% of this acceleration for Vstar.

Estimating additional C_R coefficients was also tested: instead of estimating one per satellite per arc, one can try to absorb changes in solar radiation pressure by estimating more coefficients if the data allow this. The processing software GEODYN II allows to constrain these coefficients in time by supposing a correlation function between coefficients, with a decay in correlation scaled by a correlation time. With a correlation time of 1 day, and estimating one C_R per day, with an a priori uncertainty of 10%, it was found that while this greatly improved the data fit levels, this did not uniformly improve the orbit prediction results. Estimated values for C_R showed slightly more variation, but those for Vstar improved overall, with smaller outliers.

Another way of modelling solar radiation pressure is through taking into account the complex shape of the satellite by modelling it, for example, as a set of plates (e.g., Marshall and Luthcke 1994; Luthcke et al. 1997). In SELENE, both sub-satellites are of the same hexagonal shape, with the side-panels covered by solar cells. By computing the incident solar angle, the resulting solar radiation pressure force per plate can be computed, and the net acceleration is then obtained by summing the separate vector forces. One does need to know the attitude of the satellite in inertial space for this, and since Rstar and Vstar were free-flying satellites without any other instruments apart from transponders, their attitude was not measured directly. Apart from that, reflective and absorptive properties of the satellite materials also need to be known. Orbit determination tests were done using pre-launch reflection and absorption coefficient values, together with the spin-axis direction of one of the satellites taken from the value at separation of the main satellite which was then applied to both satellites, but these tests were inconclusive: data fit and orbit prediction results did not improve. The property coefficients were also estimated from the data, but it was also found this did not lead to reasonable values for all coefficients, probably mostly due to the sparsity of tracking data (this was done without the VLBI data). The biggest uncertainty factor, however, is the attitude of both satellites. Future efforts might include trying to estimate the attitude from the raw 10 Hz Doppler data. For now, for these spinning satellites, the straightforward cannonball model gave the best results.

3.2.4 Orbit precision and data weights

Just as was done when assessing the data fit, different data weights for the VLBI data were used when computing the orbits in the prediction tests. Chosen weights were 1 cm, 1 mm and 20 cm, in order to have a wide range of data weight values. The weights for the other data were kept the same, i.e. 1 mm/s for Doppler data and 2 m for range data. The results are shown in Fig. 8. The data weight has a large effect: by changing it, orbit differences change, and in general, whether the data weight for VLBI is 20 cm or 1 mm, they get bigger. A data weight of 1 cm thus seems to be the one most appropriate, leading to the smoothest and most consistent orbit overlap differences. This is further confirmed by the results of the average RMS of orbit differences listed in Table 2. The results in this table also further show the effects of the VLBI data when their data weight is varied: by choosing 1 mm, the results for the radial direction deteriorate further, while they get closer to the Doppler and range only results for a weight of 20 cm. As in the data fit results shown in Fig. 4, this is an effect of weighted least-squares, where depending on the relative data weight, one data type will contribute more to the solution than the others as the weights shift in favour of that type.

3.2.5 VLBI data biases

As mentioned in Sect. 3.1, pass-by-pass biases were estimated for the VLBI data for each baseline. A priori uncertainties were set to 10 km, assuring a free adjustment of the parameters. The estimated bias values, collected for all baselines throughout the SELENE mission, are shown in Fig. 9. The bias values are grouped around basically three values: ± 4, ± 0.13 (see the inset in Fig. 9) and 0 m. The a posteriori uncertainties varied, depending on the strength and amount of the VLBI data available: in general, they were 2 orders smaller than the estimated values, but at times they were of the same value as the estimated biases themselves. But as Fig. 9 shows, the estimated values are consistent throughout the mission period.

Values for the estimated biases around 0 are expected, as they are small and indicate remaining media and other unmodelled effects. Values of ± 0.13 m are explained by ambiguity cycle slips of the phase delay of the S-band signal in the correlation process, since 0.13 m is the value of the wavelength of the S-band carrier (computed as 1/(2212 MHz) times the speed of light = 0.135 m). The largest outliers around ± 4 m have a similar explanation, except that they correspond with ambiguity cycle slips of the group delay: a bandwidth of 75 MHz was used for this (the span of S-band carrier frequencies used as listed in Sect. 2.2), which corresponds to a wavelength of 1/(75 MHz) times the speed of light = 3.997 m. This result was also indicated in the correlation process, where first the group delay is determined, and then the phase delay (e.g., Kono et al. 2003). Ambiguities are determined from 1 min averages, and from comparing values for these averages during an interval of 30 min

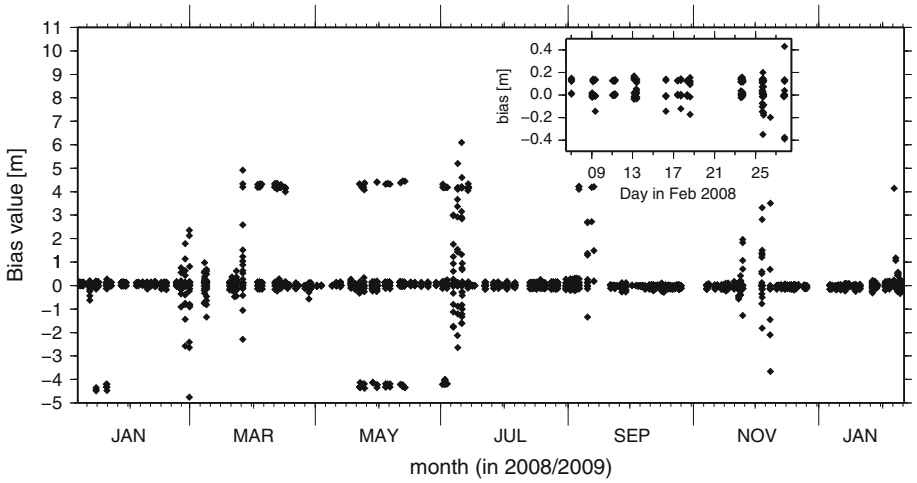

Fig. 9 Values for the estimated pass-by-pass biases per baseline on the VLBI data during the entire SELENE mission period. The *inset* shows a close-up of February 2008, showing the distribution of bias values around zero

(Kikuchi et al. 2009; Liu et al. 2010a). In the case that all values are close together, the ambiguity is fixed at that level. That might occasionally lead to cycle slips. And if one occurs for the determination of the group delay, then that also affects the phase delay. The ambiguity determination for the phase delay part will then show large variations for the 30 one-minute intervals, since one group delay cycle equals about 30 phase delay cycle slips (2212/75). And indeed it was found that in several reoccurring cases, the phase delay ambiguity could not be determined well, with differences of 30 cycles between the one-minute averages (during a 30 min interval). This occurred mostly for the Ogasawara station, and again for some of the longer baselines. The ±4 m outliers for the estimated bias values were traced back to these instances, for precisely these stations or baselines. It is thus reassuring that even if cycle slips occur in the correlation processing, they can be absorbed by estimating biases on the data.

Finally, the internal consistency of biases per baseline was tested. In Kikuchi et al. (2009) and Liu et al. (2010a) the closure phase of the VLBI data was investigated. This is the signed sum between three baselines that form a closed triangle. If the delays are summed with the appropriate sign, the total delay should be zero, since effectively a delay at one and the same station is computed. A similar test was done here on a sample subset of the estimated biases: signed-sums were indeed found to be much smaller than the separate biases per baselines, indicating consistency between the estimated biases, without constraining them to behave in that way.

3.3 Summary

Orbit determination precision has been assessed by means of the analysis of orbit differences during an overlapping period of two consecutive arcs, where the first arc is propagated (without the use of data) to overlap with the next arc. Including VLBI data greatly improves the orbit consistency, from a few hundred metres when using Doppler and range data only, to a few tens of metres when including VLBI data. A data weight of 1 cm for the VLBI data in the orbit determination gives the best, most consistent orbit differences, while retaining good level of post-fit residuals for all data involved. Solar radiation pressure was found to be modelled best by a simple cannonball model. The estimated biases on the VLBI data were shown to be related mostly to ambiguity cycle slips.

4 Lunar gravity field determination with VLBI data

The results from orbit determination as described above were used in lunar gravity field determination including the VLBI data. Historical tracking data, meaning data from satellites prior to SELENE, were also included. This section describes both the processing and the results.

4.1 Tracking data processing

The lunar gravitational potential U is modelled as a spherical harmonics expansion with normalised coefficients following Kaula (1966):

$$U(r,\lambda,\phi) = \frac{GM}{r}\sum_{l=0}^{l_{\max}}\left(\frac{a_e}{r}\right)^l \sum_{m=0}^{l}\bar{P}_{l,m}(\sin\phi) \times\left(\bar{C}_{l,m}\cos m\lambda + \bar{S}_{l,m}\sin m\lambda\right) \quad (2)$$

where r, λ, ϕ are the spherical coordinates radius, longitude and latitude, respectively, GM is the lunar gravitational parameter, a_e the reference radius (1738.0 km), $\bar{C}_{l,m}$ and $\bar{S}_{l,m}$ the normalised Stokes coefficients of degree l and order m that are to be determined, and $\bar{P}_{l,m}$ are the normalised associated Legendre polynomials.

For the determination of the spherical harmonics coefficients, normal matrices per arc are generated, aggregated over all arcs, and then the parameters are estimated. Normal

matrices contain in general both common and arc parameters, and through a partitioning scheme (e.g., Kaula 1966) the arc parameters can be eliminated, leaving only the common parameters to be estimated. Normal matrices per arc are generated from orbit determination runs: first the arc parameters are adjusted until convergence is reached, keeping the global parameters fixed to their a priori values, and then the partials of the data with respect to all the parameters (both arc and common) are computed and summed into the normal matrix for that arc. That means that in principle with the precise orbit determination results from the previous section, normal matrices for gravity field determination can be readily made by writing out partials to the desired parameters.

However, for SELENE it is more complicated than that because of the data types involving different satellites: the 4-way data tie the main orbiter to Rstar, while the VLBI data tie Rstar to Vstar. In order to determine the lunar gravity field using these data types, multi-satellite arcs must thus be created. Initially, orbit determination results described in the previous section were only between Rstar and Vstar because the 4-way data were not used yet.

How to use the 4-way data in gravity field determination has been described extensively in Matsumoto et al. (2010), so the reader is referred there for most of the details. Gravity field determination results here follow that strategy, with the only difference that Rstar and Vstar arcs are now longer, and tied together. Arc length is nominally 1 week, although there are periods where Vstar's arc is extended to 2 weeks, from results in Fig. 7. Arcs for the main orbiter remain limited to 12 h until July 23, 2008, and are shortened to on average 6 h afterwards, due to angular momentum desaturation events on-board the main satellite. Using the decided arc length for the R/Vstar combination, that period is then filled up with consecutive arcs of the main satellite. Since the orbit determination described in the previous section was performed with the goal to use later the same arcs for gravity field determination, care was taken not to have Rstar arcs start or end in the middle of a 4-way pass so as not to disrupt them. The orbits for all the satellites in one arc were iterated to convergence using all the data types simultaneously, after which the normal matrix for gravity estimation was generated. This, as well as the orbit fitting part, was done using GEODYN II, while the normal matrices are aggregated with the accompanying software package SOLVE (Ullman 2002), which was also used for determining the parameters afterwards.

The arc parameters that were estimated were the state vectors of all satellites involved, one solar radiation pressure coefficient C_R per arc per satellite, empirical accelerations for Rstar and Vstar as described in the previous section, and biases on the following data types: all 2-way range data, 2-way Doppler for R/Vstar due to spin, VLBI data and 4-way data [see Matsumoto et al. (2010) for specifics of the 4-way biases]. Estimated common parameters were the Stokes coefficients of the spherical harmonics expansion of the lunar gravity field up to degree and order 100, the lunar gravitational constant GM and the lunar degree 2 potential Love number k_2. Force and measurement modelling was the same as in the processing of the SGM100h model, except that now the a priori field was SGM100h itself.

The chosen data weights for all Doppler and range data were also the same as in the processing of SGM100h, i.e. 1 mm/s for 4-way Doppler data, and 2-way Doppler data from UDSC, 2 mm/s for 2-way Doppler data from the other stations (for the main orbiter) and 5 m for the 2-way range data. Following the orbit determination results, it was chosen to have the VLBI data weighted at 1 cm: the post-fit residual was at or below this level, as shown in Fig. 5, and the orbit prediction results were most consistent for this data weight, as Fig. 8 showed. Considering that the intrinsic noise level for the VLBI data was estimated to be around a few mm, depending on the frequency band and separation angle (Kikuchi et al. 2009; Liu et al. 2010a), the data are slightly downweighted. This is the case for all data, as Doppler data also typically have a better accuracy than 1 mm/s [see for example Konopliv et al. (2001) for discussions about Lunar Prospector]. Downweighting is done often in order to allow for remaining errors due to the mismodelling of media effects and spacecraft dynamics (e.g., Border et al. 1992). The influence on the estimated covariance will be discussed later in Sect. 5.

Historical tracking data, referring to satellites before SELENE in this case, were also included. This comprises tracking data from the Lunar Orbiters (LO) I–V, the Apollo 15 and 16 sub-satellites, Clementine, Lunar Prospector's (LP) nominal mission data (taken in 1998) and some SMART-1 data. Similar to the processing for SGM100h, the LP extended mission data are left out, because it was felt that they contain too much information beyond degree and order 100, and they would thus disrupt the gravity field over especially the far side too much, although they remain extremely valuable for future efforts using models with larger expansions. Another reason is of course to have a better comparison with SGM100h to assess the influence of the VLBI data and longer arc lengths for R/Vstar, which is also why the data weights for data types other than the differential VLBI data (including historical tracking data) were kept the same. The historical mission data are described excellently in Konopliv et al. (1993) and Lemoine et al. (1997), and the LP data in Konopliv et al. (2001). Processing of these data were exactly the same as in Matsumoto et al. (2010).

SELENE solutions can be estimated up to degree and order 70 without the use of a priori information (Matsumoto et al. 2010). However, for reasons similar to those for SGM100h (i.e., suppression of excessive power in coefficients of degree and order higher than 70, resulting from a remaining gap in 4-way tracking data coverage over the northern far side), it was chosen here to use a Kaula rule to smooth the gravity field

coefficients, although unregularised solutions up to degree and order 70 can also be constructed. This rule consists of constraining the coefficient values towards zero with an uncertainty given by $\sigma(\bar{C}_{l,m}, \bar{S}_{l,m}) = \beta \times 10^{-4}/l^2$. The constant β was chosen here to be 3.6, in accordance with previous studies (Lemoine et al. 1997; Konopliv et al. 2001; Matsumoto et al. 2010).

4.2 Gravity determination results

Gravity field determination as described above has resulted in a gravity field model that is designated as SGM100i. The Stokes coefficients of this model, together with the VLBI data files, can be obtained from the RISE Data archive website located at http://www.miz.nao.ac.jp/rise-pub/en or from the SELENE Data archive website at http://www.soac.selene.isas.jaxa.jp/archive/. There are various ways of assessing the results, for example through formal errors for the coefficients, examination of the resulting gravity anomalies, correlations between gravity and topography and performance in orbit determination. The focus here will mostly be on comparing SGM100i and SGM100h and thus in establishing the influence of the VLBI data. More discussion on the results will be given in the next section.

4.2.1 Power of the coefficients

Figure 10 shows the degree-wise RMS spectral power amplitude for both the coefficients and associated errors for SGM100h and SGM100i. The degree-wise RMS amplitude

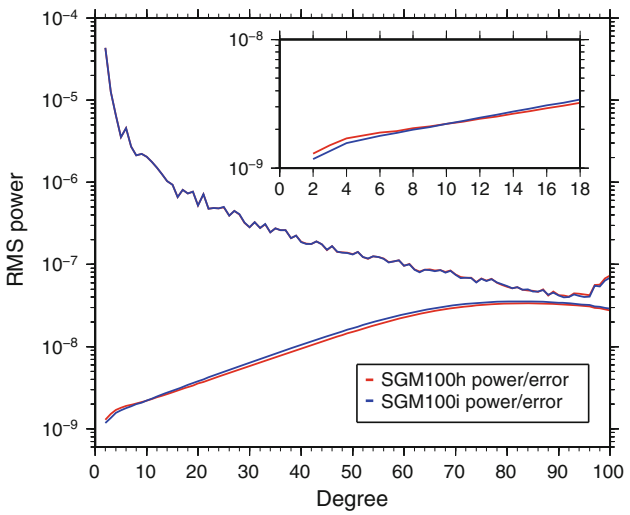

Fig. 10 Degree-wise RMS spectral power amplitudes for both the coefficients (labelled "*power*") and their associated errors (labelled "*error*") for both SGM100h and SGM100i. The *inset* shows a close-up for the lower degrees

σ_l is computed from

$$\sigma_l = \sqrt{\frac{\sum_{m=0}^{l}(\bar{C}_{l,m}^2 + \bar{S}_{l,m}^2)}{2l+1}} \tag{3}$$

where the amplitude for the associated errors is computed by using the formal errors for the coefficients, which are taken from the diagonal of the covariance matrix. The figure shows very few differences in the RMS power between the two models, suggesting that they are nearly similar. The formal errors, however, are slightly different. Due to the longer arc lengths and the precise VLBI data, it is expected that the VLBI data mostly contribute to the lower degrees, up to about 20 (Matsumoto et al. 2008). With formal errors only slightly lower for the lower degrees, Fig. 10 confirms this, but the improvement in formal error is only marginal. Further discussion focusing on the lower degrees is given in the next section, but it can already be said here that the final model was chosen based on a number of criteria, such as data fit and orbit prediction results, and because of this, several VLBI arcs and a portion of Vstar-only arcs were excluded, leading to increases in the formal errors for the lower degrees.

4.2.2 Gravity anomalies and associated errors

Gravity anomalies at the reference surface (a sphere with a radius of 1738 km) are plotted in Fig. 11. These anomalies again show clearly the far side circular basins, but differences with SGM100h are difficult to spot, which was also concluded from inspecting the degree-wise RMS spectral amplitudes in Fig. 10. Hence, the differences in anomalies between SGM100h and SGM100i are also shown in Fig. 11. The minimum, maximum and RMS value of the differences were -151, 161 and 21 mGal, respectively (1 mGal $= 10^{-5}$ m/s^2). The largest differences are concentrated over the northern far side, where the 4-way Doppler coverage was lower, due to Rstar's apolune being located over the southern hemisphere (Matsumoto et al. 2010). It is thus likely that the differences in the north part of the far side mostly stem from the effects of the ill-posed inverse problem, and that they show the influence of the used Kaula rule, since this is likely to manifest itself most clearly in parts less covered (and thus less constrained) by data. This means one should be careful to use these models for geophysical interpretation in this part of the far side, at the smaller scales. Differences in other parts, like the southern far side and the poles, are more likely to be due to the influence of the different processing such as longer arc lengths of Rstar and Vstar, made possible by the inclusion of VLBI data. However, the differences by themselves cannot indicate whether there is an improvement.

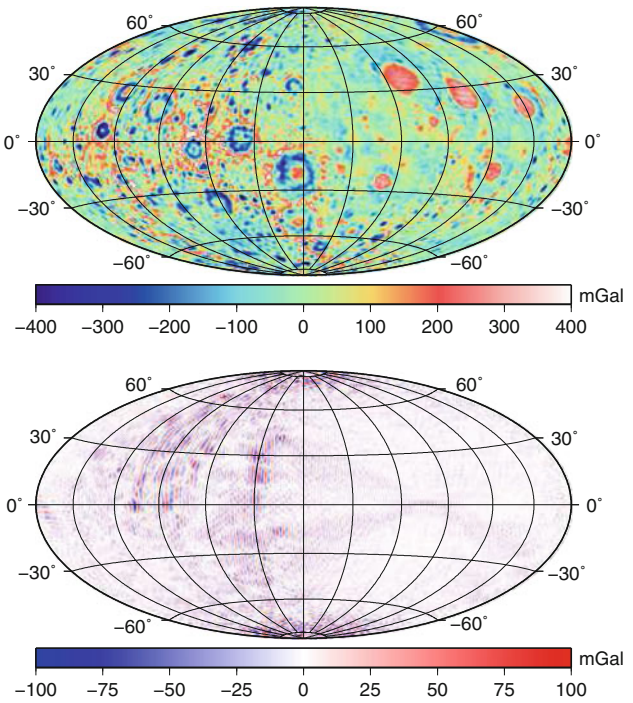

Fig. 11 Gravity anomalies at the reference surface (a sphere with a radius of 1738 km), computed in spherical approximation, for the SGM100i model (*top*). Differences between SGM100i and SGM100h are also shown (*bottom*). The minimum, maximum and RMS of the anomaly differences are −151, 161 and 21 mGal, respectively. The projection for both plots is the same as that used for Fig. 2

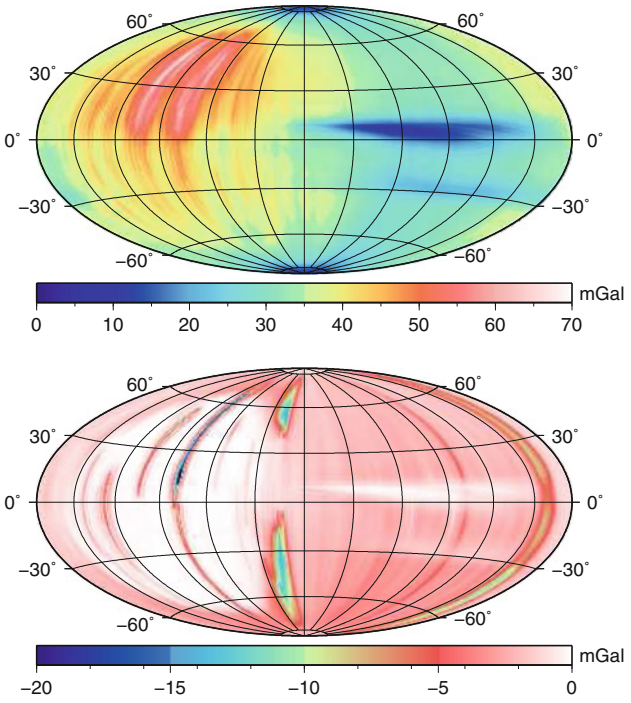

Fig. 12 Anomaly errors at the reference surface computed from the full covariance matrix, for SGM100i (*top*). The differences in covariance, computed as error(SGM100h)–error(SGM100i), are shown in the *bottom plot*. Negative anomaly error differences thus mean a larger projected error for SGM100i

In addition to the gravity anomalies, the projected errors in gravity anomalies at the reference surface as computed from the full covariance matrix can also be investigated. For comparison, both the anomaly errors from SGM100i covariance and the difference between anomaly errors computed as error(SGM100h) − error(SGM100i) are given in Fig. 12. On average, the anomaly errors are 2.24 mGal higher for SGM100i. The biggest differences occur at the limb areas (an area of about ±10° around 90° and 270° eastern longitude), where for SGM100i the anomaly errors are higher (negative differences in the difference plot). This is somewhat surprising, as the VLBI data are at least expected to contribute positively to especially the determination of the gravity field over the limb areas, due to a better sensitivity to satellite position when compared to 2-way data for orbits covering those areas (where the angle between line-of-sight and the orbital plane is close to 90°). The increase in anomaly errors as computed from covariance, which is also clear from the higher RMS power of the associated errors for SGM100i with respect to SGM100h as shown in Fig. 10, is likely due to the longer arc lengths for Rstar and Vstar used in the processing. This will be discussed further in the next section. Data coverage in general, as shown in Fig. 2, corresponds to differences in anomaly errors, for example for tracks on the far side and over the limbs.

4.2.3 Correlations with topography

Correlations between gravity and topography are another way to evaluate the gravity model: improved correlations between the two are in general thought to show improvements in either topography or gravity, as especially at the higher degrees, uncompensated topography should be reflected in the gravity field. The topography model used here is an expansion in spherical harmonics up to degree and order 359, called STM-359_grid-03 and has been derived from SELENE laser altimeter data. It is an updated version of the model presented in Araki et al. (2009). Global correlations between SGM100i and STM-359_grid-03 hardly differ from correlations between SGM100h and STM-359_grid-03. Because the gravity differences were located over the far side, localised correlations over the far side are computed (e.g., Wieczorek and Simons 2005). These are shown in Fig. 13. SGM100i shows higher correlations for higher degrees. As stated earlier, anomaly differences in the northern far side are likely due to the effects of the ill-posed inverse problem. However, localised correlations are computed here over the whole far side area.

Compared with SGM100h, SGM100i consists of another iteration over the whole data set. Nevertheless, increased correlations are not thought of as an artefact of an extra iteration (where extra information is extracted from the data through

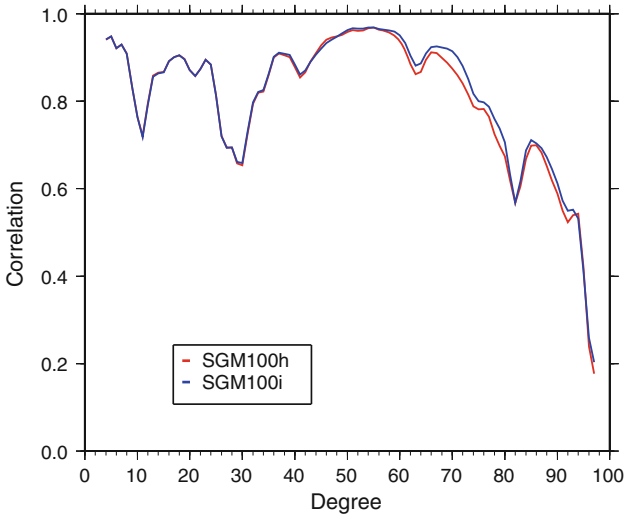

Fig. 13 Correlations between topography and gravity, localised over the far side

reprocessing), because the increase in correlations between SGM100h and its predecessor model are not as large as those shown in Fig. 13. This means that the increase is likely to stem from the different processing using different arc lengths.

4.2.4 Data fit and orbit determination performance

The new model has also been tested for orbit determination performance, by computing data fit and orbit predictions for a test period of Lunar Prospector arcs in its nominal mission period. The arcs for LP were 2 days long, like in the gravity field determination processing, and for the orbit predictions, the orbit was propagated for 1 day, and then differenced with a consecutive arc. The results for SGM100i are compared with those for SGM100h and LP100K, the latter of which is a pre-SELENE 100th degree and order spherical harmonics expansion of the gravity field based on the complete Lunar Prospector data set, including the extended mission data (Konopliv and Yuan 1999).

Data fit results presented in Fig. 14 show that on average, SGM100i has a better (lower) data fit. It is also more consistent, as some of the peaks that were both visible in results for LP100K and SGM100h are smaller. These data fit peaks often coincide with edge-on orbits, where the satellite covers the deep far side. Orbit prediction results are shown in Fig. 15. Although there are instances for which SGM100h or LP100K have a better performance, in general SGM100i produces the smallest orbit overlaps. Similar to what was shown in the plot for the data fit, especially the peaks in the orbit differences are smaller. Results for SGM100h showed that this model often performed better than LP100K in edge-on orbits due to inclusion of the far side tracking data (Matsumoto et al. 2010). This is corroborated by the results shown here: there are further improvement for edge-on orbits for SGM100i, compared with SGM100h. These orbits are over the deep far side, the part of the gravity field that showed the largest differences with SGM100h. On top of that, there are also improvements for some of the face-on orbits, where the satellite flies over the limb areas of the Moon, although those improvements are much less drastic than the reduction of the peak values for the edge-on orbits. As pointed out earlier, the SGM100i model has larger anomaly errors in these areas. Table 3 shows the average RMS of orbit differences in the local satellite orbit frame, and this allows to further investigate differences between the results using various models. This table shows that the results for the three models are all similar, but that SGM100i further improves the along and cross track directions, up to a total orbit error now less than 30 m, while it was 36 m for LP100K.

The performance of the new model for the VLBI arcs that were used in the gravity field processing is assessed through RMS of data fit values. Post-fit values from processing the VLBI arcs with the newly determined SGM100i model are compared with the residuals prior to the gravity field inversion and with post-fit residual levels as reported

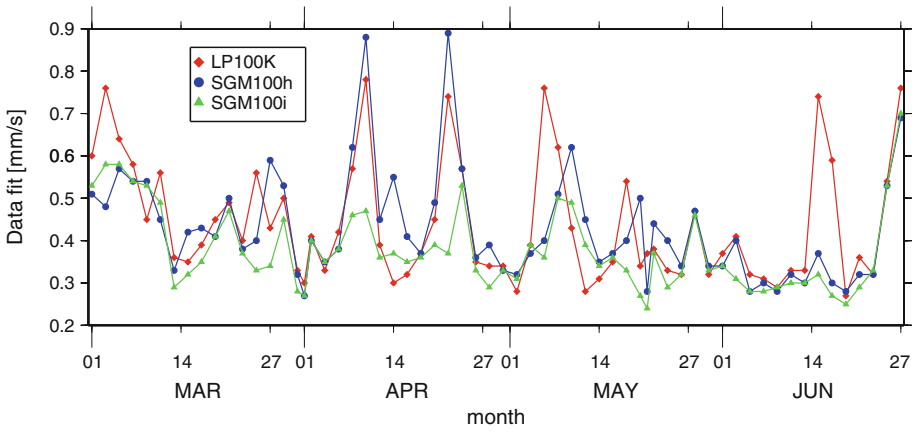

Fig. 14 RMS of Doppler data fit for 2-day arcs for Lunar Prospector in 1998, for various models

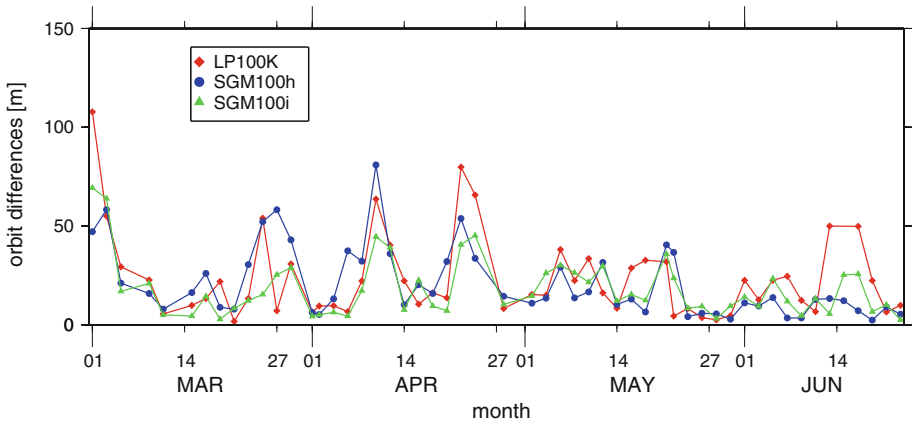

Fig. 15 Root-sum-square of overlap differences for 1-day orbit predictions from 2-day Lunar Prospector data arcs, for various gravity field models

Table 3 Average values for the RMS of orbit differences for 1-day orbit predictions from 2-day arcs of Lunar Prospector data (as presented in Fig. 15), separated per direction in the local satellite orbit frame

Model	Orbit differences (m)			
	Radial	Along	Cross	Total
LP100K	1.06	27.36	16.86	35.93
SGM100h	1.19	24.19	13.33	31.65
SGM100i	1.05	23.07	11.38	29.15

Table 4 Post-fit RMS values per data type per satellite for the VLBI arcs, before and after gravity field determination

Data type and satellite	SGM100h	Before gravity determination	After gravity determination
VLBI data	–	0.666	0.508
Rstar Doppler	0.50	0.236	0.167
Rstar range	158.0	86.976	75.273
Vstar Doppler	0.18	0.676	0.239
Vstar range	103.0	152.375	95.561
Main Doppler	0.770	0.779	0.771
Main range	82.0	24.266	23.564
4-way Doppler	0.48	0.438	0.396

For comparison, post-fit RMS values for residuals taken from Matsumoto et al. (2010) are also listed, labelled "SGM100h". The difference with the results from before gravity determination is the use of VLBI data and the longer arc lengths in the processing. Units are cm for range data types (2-way range and VLBI) and mm/s for Doppler data types

in Matsumoto et al. (2010) using SGM100h. The difference between those and the residuals prior to gravity inversion here is the use of VLBI data and the accompanying longer arcs. The RMS of data fit values are listed in Table 4. As expected, the data fit is improved for the new model, since this model was based on the arcs used to compute the data fit values. The values for data fit for Vstar seem to benefit most from using the VLBI, when comparing the results of before and after gravity field determination, which is not that surprising considering the few 2-way tracking data available for that satellite. The results for Vstar in the SGM100h processing gave a better data fit due to the shorter arc lengths used there. Interestingly, the 4-way fit is better when using the VLBI data, both before and after gravity inversion, although the differences are not big. This can indicate a better positioning for Rstar using the VLBI data, leading to a better residual on the 4-way data. Range data types also benefit from using the VLBI data. Redoing the orbit prediction analysis presented in Sect. 3.2 (in Fig. 7) with SGM100i (thus reprocessing the VLBI arcs with a gravity field model that was derived using those same arcs) showed further orbit prediction improvements for Rstar and Vstar: both are at a level of 20 m, when including the VLBI data in the analysis.

4.2.5 GM and k_2 values

The lunar gravitational parameter GM and the degree 2 potential Love number k_2 were also estimated. The value for GM did not change much with respect to SGM100h, with a result of $GM = 4902.80080 \pm 0.00009$ km^3/s^2 for SGM100i, versus $GM = 4902.80212 \pm 0.00013$ km^3/s^2 for SGM100h. The listed errors are 1 sigma. The differences between the GM values for SGM100h and SGM100i are still at a 10-sigma level, but interestingly, the value for SGM100i is closer to that from the DE421 ephemeris, which is 4902.80008 ± 0.0001 km^3/s^2 (Williams and Boggs 2008). The difference is about 8 sigma.

The lunar degree 2 potential Love number k_2 is an important parameter because it can be used to constrain models of the lunar interior structure (Williams et al. 2001; Wieczorek et al. 2006). The use of SELENE far side data, and the use of longer arc lengths for the sub-satellites, is expected to contribute to decreasing the uncertainties in the k_2 value (Goossens and Matsumoto 2008; Matsumoto et al. 2010). The value for k_2 for SGM100h was 0.0240 ± 0.0015, and the value for k_2 for SGM100i is a little higher, at 0.0255 ± 0.0016. The listed errors for k_2 are ten times the

formal error, following Konopliv et al. (2001) to allow for optimistic formal errors from covariance. There is thus not much change in either the value or error on k_2 when compared with SGM100h. The discrepancy with the value from lunar laser ranging (LLR), $k_2 = 0.0209 \pm 0.0025$ (Williams et al. 2010), still exists, and the uncertainty is not below the 5% level needed to be able to distinguish the effects of the presence of an iron core (Wieczorek et al. 2006). More discussion on the value for k_2 and its correlation with gravity coefficients is given in the next section.

5 Discussion

The higher correlations with topography over the far side, the better data fit and the better orbit prediction results for especially the edge-on orbits show that SGM100i shows improved performance for these different qualities when compared with SGM100h. Yet, results such as the marginal improvements in formal error for the lower degrees, larger anomaly errors over the limbs and a slight increase in the formal error for the degree 2 potential Love number k_2 show that the influence of the VLBI data is not as straightforward as perhaps initially expected. Instead, the influence of the VLBI data on the solution is more subtle, not necessarily limited to the lower degrees through the orbits of Rstar and Vstar and their intrinsic gravitational sensitivity, but also showing itself in higher degrees, through Rstar's orbit's influence on the 4-way data.

5.1 Limb areas

As mentioned earlier, the VLBI data are expected to contribute to the gravity field over the limb areas because of their additional orbital sensitivity, when compared with 2-way data alone. For SELENE however, there were also the 4-way data, and some of them were taken over the limb areas, adding a radial sensitivity to the gravity field in those areas (Matsumoto et al. 2010). The higher anomaly errors for the limb areas for SGM100i thus should not be seen as an unexpected negative side effect of the VLBI data, but rather, as stemming from a decrease in contribution from the 4-way data, likely due to the longer arc lengths used. This was further corroborated by inspection of intermediate results using 1 week arcs but without the VLBI data. Plots of anomaly errors from covariance then show signals similar to those in Fig. 12, showing that the increase in anomaly error is an effect of increasing arc length of Rstar that cannot be completely undone by including VLBI data. But more importantly, the slightly improved orbit consistencies over the limbs show that the model performs better, despite the higher anomaly errors from covariance, which points to calibration issues of the lunar gravity field models (see also later when the lower degrees are discussed in this section).

The influence of the 4-way data on the limbs can also be investigated in another way: when the localised correlations between gravity and topography are computed over the Mare Orientale region on the eastern limb of the Moon (results not shown here), SGM100h shows improved correlations when compared with LP100K. There are some further improved correlations between SGM100i and SGM100h but they are only minor, showing that most of the improvements between SELENE models and previous models come from the 4-way data for this area.

5.2 Lower degrees

By including VLBI data it has been possible to extend the arc lengths for Rstar and Vstar, and through this it is reasonable to expect improvements in especially the lower degrees and orders of the gravity field expansion, since they mostly drive the long-term changes in the orbit. Such improvements were shown for example in pre-mission simulations (Matsumoto et al. 2008). However, inspection of the formal errors as depicted in Fig. 10 has shown only a marginal improvement. One thing already mentioned in the previous section is the final data selection for computing SGM100i. In the gravity processing, results per arc were inspected for data fit, and overlaps in between arcs. Inversions were done with the full set of VLBI arcs and a subset where some arcs were excluded, on the basis of higher VLBI residuals (close to Rstar's end-of-life), or relatively high overlaps (one arc in December 2008, excluded from Fig. 7). All inversions used all other data, both historical and SELENE tracking. Resulting models were then evaluated for orbit predictions with LP data (Fig. 15) and consistency of the moment of inertia (see below). It was found that the subset solution performed best in all respects, yet this does mean leaving out a small part of the data. Formal errors for the inversion with the full set were lower. This might be interpreted as a hint that the improvement in lower degrees is only due to including more data (though not that much, compared with the amount of 2-way data), but this is not the case: the shape of the RMS power spectrum of the associated coefficient errors for SGM100i is distinctly different, showing that there is an influence from the longer arcs, made possible by the VLBI data.

However, even longer arcs are probably necessary to improve the gravity field coefficients of especially the lower degrees. The pre-mission simulations described in Matsumoto et al. (2008) used an arc length of 2 weeks, and assumed perfectly known orbits for the sub-satellites. Experience with processing the data shows that these expectations cannot be met. Overlap analysis with 2 week arcs instead of 1 week arcs showed worse results for the former, after which 1 week arcs were selected. And despite the improved

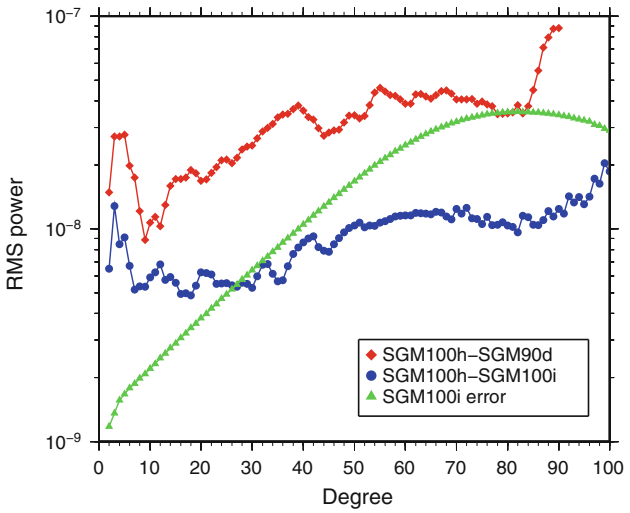

Fig. 16 Degree-wise RMS spectral power amplitudes according to Eq. (3) for differences in coefficients between several models. For comparison, the formal errors for SGM100i are also plotted

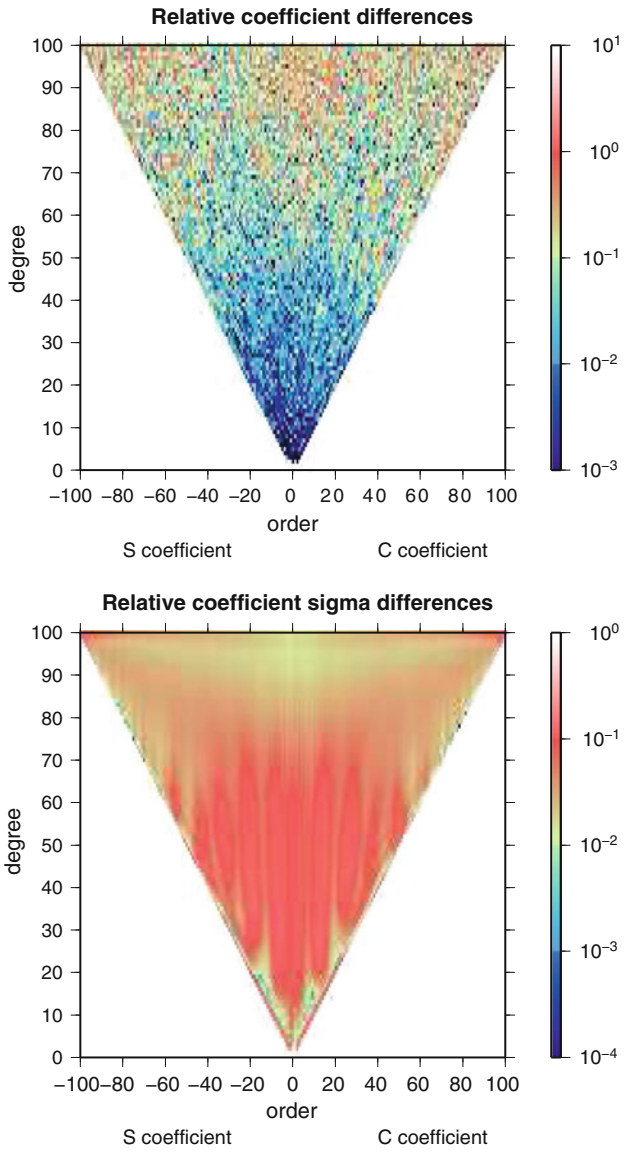

Fig. 17 Relative differences between SGM100i and SGM100h for the coefficients of the spherical harmonics expansion (*top*) and their associated errors (*bottom*)

orbit consistency when the VLBI data are included, there are remaining orbit errors on the sub-satellites, cf. Fig. 7. This, thus, has lead to a smaller improvement in formal errors for the lower degrees than initially expected. Care should be taken, however, not to attach too much meaning to the results for the formal errors. Calibration of lunar gravity field models remains a delicate issue (see Floberghagen (2002) for a good discussion, and also Mazarico et al. (2010) for a recent example). It is not uncommon to add a safety factor to gravity uncertainties computed from the a posteriori covariance matrix such as shown in Fig. 12. In the case of LP, Konopliv et al. (2001) uses a factor of 2, which can be applied here as well, because it matches the observed differences shown in Fig. 11 with the aforementioned uncertainties. This indicates that the current formal errors on the SGM solutions might be over-optimistic, perhaps due to tight data weights (Floberghagen 2002), despite downweighting the data as was discussed in Sect. 4.1. Note also that in the RMS spectral power plot in Fig. 10, the error never reaches the signal.

Results in Matsumoto et al. (2010) also showed the difficulties in determining the lower degree and order coefficients precisely, by investigating coefficient differences between models and plotting the degree-wise RMS spectral amplitudes for them. The same is done here in Fig. 16, by comparing differences between SGM100h and the earlier model SGM90d (Namiki et al. 2009), with differences between SGM100i and SGM100h. The formal errors for SGM100i are also included. The figure shows that for the lower degrees the coefficients are indeed difficult to determine, since the differences for these coefficients are still larger than the formal errors. However, these differences are smaller than those between previous SELENE-based models. The RMS spectral amplitudes for the higher degrees show a much flatter signal, well below the $1-\sigma$ error of SGM100i. But moreover, the differences in the lower degrees between SGM100h and SGM100i shown in this figure indicate the actual differences between the models due to data and processing, rather than due to the effects of the ill-posed inverse problem, which are expected to be in the higher degrees. Despite only a small improvement in formal errors, this does show that the lower degrees are affected. Differences from the lower degrees are difficult to see in plots of surface gravity anomalies such as shown in Fig. 11. These differences likely contribute to the improved orbit and data fit results for SGM100i when compared with SGM100h.

5.3 Coefficient differences

One other way to compare SGM100h and SGM100i is to have a direct look at the coefficient differences, to see which coefficients are affected by the inclusion of the VLBI data, and the longer arc lengths of the sub-satellites. Figure 17 shows the relative coefficient differences for both the spherical harmonic coefficients and their associated errors. These relative differences $\delta\{\bar{C}, \bar{S}\}_{l,m}$ are computed as

$$\delta\{\bar{C}, \bar{S}\}_{l,m} = \left| \frac{\{\bar{C}, \bar{S}_{l,m}\}_{\mathrm{SGM100i}} - \{\bar{C}, \bar{S}_{l,m}\}_{\mathrm{SGM100h}}}{\{\bar{C}, \bar{S}_{l,m}\}_{\mathrm{SGM100h}}} \right| \quad (4)$$

The relative coefficient differences show a large spread: the smallest deviation is in the order of 10^{-6} for $\bar{S}_{33,11}$, and the largest deviation is in the order of 300 for $\bar{C}_{49,42}$. Figure 17 shows that most differences are in the higher degrees and orders, which is translated in the difference plot of Fig. 11 into the high-frequency differences. This is also where the largest differences are expected, due to the effects of the ill-posed inverse problem, as discussed earlier. Figure 17 also shows some differences for some of the lower order and degree coefficients, which was also clear from Fig. 16.

The relative differences for the associated errors carry information about how well the coefficients are determined, relatively between the two models. Inspection of the sign of the relative coefficient sigma errors, where a negative value would mean a smaller associated error for that particular coefficient of SGM100i versus SGM100h, shows that some of the lower degree coefficients together with the sectorial terms ($l = m$) have a smaller sigma. The clear signal in the plot for the errors in Fig. 17, where a band of orders close together are grouped, showing an enhanced coefficient sigma between SGM100i and SGM100h (although the relative difference is in the order of 0.1), is likely to represent the influence of using longer arcs for the sub-satellites. Note also that the range of degrees with this signal is similar to that in Fig. 10 where SGM100i had a higher RMS of power in the associated errors than SGM100h. Although the broad groups of orders with enhanced errors stand out in Fig. 17, alternatively, the isolated smaller bands of orders can be thought of as representing that part of the processing between SGM100h and SGM100i that was the same, which is mainly the historical data. The biggest changes occur up to about order 60, which is equivalent to orbital periods of about half a day. This follows from linear perturbation theory (LPT) that relates orbital perturbations to the spherical harmonics coefficients of the gravity field expansion (e.g. Kaula 1966), showing that an order m induces perturbations with a period of 1 month over m, the m-monthlies [see also Floberghagen (2002) for further discussion]. Half a day is the arc length of the main orbiter of SELENE.

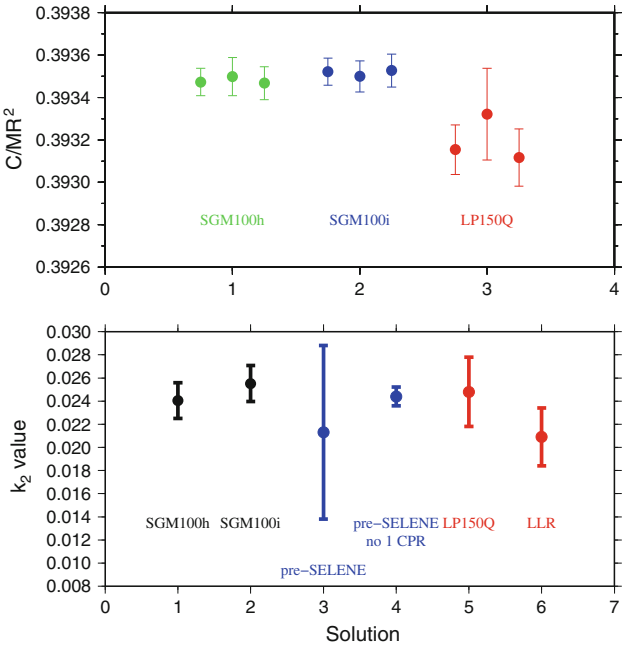

Fig. 18 Values for the lunar normalised polar moment of inertia C/MR^2 (*top*) and degree 2 potential Love number k_2 (*bottom*) for various solutions. Errors for k_2 are based on ten times the formal error, while errors for C/MR^2 are based on five times the formal errors for gravity coefficients

5.4 Moment of inertia and lunar Love number

The consistency of the moment of inertia was also mentioned as a criterion against which models were evaluated. Moments of inertia give information about the state of differentiation of a body, and they can be computed from the gravity coefficients J_2, $C_{2,2}$ and the librational parameters β and γ (e.g., Williams et al. 2001). This gives four constraints on the three principal moments of inertia, making it possible to use different subsets of parameters to compute them. In Bills (1995) it was shown that for pre-LP lunar gravity field models, the results for the moments of inertia varied more than 15 times the formal errors, depending on which subset was used. Subsequently, in Konopliv et al. (1998) it was reported that with the LP data the variation disappeared. When processing the SELENE data, however, it was found that variations still existed, although they were much less than 15 times the formal errors. Internal consistency of computed moments of inertia was thus adopted as another evaluation criterion. Figure 18 shows results for both the lunar degree 2 potential Love number k_2 and for the normalised polar moment of inertia C/MR^2 with M the mass of the Moon and R the radius. The polar moment of inertia was computed following the equations given in Bills (1995), using values for β and γ from Konopliv et al. (1998). There are four different ways of computing C/MR^2, but two of them lead to the same

equation, so Fig. 18 only shows the three different results. Results for k_2 are also included, as corrections to the derived gravity field coefficients J_2 and $C_{2,2}$ are needed to make everything consistent for rigid values; see Williams et al. (2001) for how to correct. In the plot for k_2, pre-SELENE results come from Goossens and Matsumoto (2008) and from Konopliv et al. (2001) (denoted LP150Q, which is the name of a 150th degree and order lunar gravity field model based on processing presented in the quoted reference). For comparison, one result based on LLR is also included, coming from Williams et al. (2010). Pre-SELENE processing explored various parameterizations for processing the data, and the current SELENE processing, for both SGM100h and SGM100i, does not use empirical accelerations in the processing of LP (as labelled by "pre-SELENE, no 1 CPR" in Fig. 18).

Results in Fig. 18 show that both SGM100h and SGM100i have values for C/MR^2 that are very consistent, even more so than those for LP150Q. Other inversions using the VLBI data, for instance using the full set as mentioned earlier, resulted in more scatter in the results for C/MR^2. That scatter was mostly caused by the $C_{2,2}$ coefficient: one way for computing the moment of inertia is given as $C/MR^2 = 4C_{2,2}/\gamma$, and it was always this value that produced the outlier. By deleting arcs with outlying overlap results, the consistency of C/MR^2 was found to be greatly improved. However, Fig. 18 also shows that results from both SGM100h and SGM100i give a substantially higher C/MR^2; the value for SGM100i is 0.39351 ± 0.00007 (based on five times the formal error for the gravity coefficients) and that for SGM100h is 0.39348 ± 0.00008, compared with 0.3932 ± 0.0002 for the LP models (Konopliv et al. 2001). The result for k_2 for SGM100i is also slightly higher than that for SGM100h. Due to the corrections made on the J_2 and $C_{2,2}$ coefficients using k_2, the latter also influences the moment of inertia. Seeing as SGM100i gives high values for both C/MR^2 and k_2, there can be a coupling between them. Inspection of correlations between k_2 and gravity field coefficients showed that k_2 has the highest correlations with $C_{2,2}$, for both SGM100h (-0.29) and SGM100i (-0.41). Such correlations between k_2 and $C_{2,2}$ were also found in the pre-SELENE analysis (Goossens and Matsumoto 2008). There, the use of empirical accelerations for the LP processing influenced the results for k_2, in terms of both its value and its correlation with gravitational parameters. For the processing of SGM100h and SGM100i, empirical accelerations were not applied to LP, but they were used for Rstar and Vstar, which might influence the results. As stated in Sect. 3.2, not including the empirical accelerations resulted in larger orbit differences. Excluding them from the gravity processing as well results in a gravity field model with a drastic loss of correlation between gravity and topography over the far side, and even larger correlations between k_2 and the gravity field coefficients $C_{2,0}$ and $C_{2,2}$, of 0.13 and -0.53, respectively. This could very well point to a separability issue between these parameters. At an arc length of 1 week, there should be a better sensitivity with respect to especially the lower orders, following again from LPT and the m-monthly signal.

The pre-SELENE analysis presented in Goossens and Matsumoto (2008), and results from inversions with SELENE data still show that LP data are of great importance for the lower degrees. Despite the relatively short arc lengths that can be achieved for these data, the data are continuous during the arcs. By stacking arcs covering a long period with almost continuous data coverage, the lower orders and degrees can be resolved up to certain precision. It is expected that with the current SGM100i model, arc lengths for LP can be extended, due to inclusion of both the far side and VLBI data that can both help to limit dynamical error build-up, and that might lead to further constraints on the lower degrees and Love number k_2.

6 Conclusions and outlook

All same-beam S-band differential VLBI data collected in the SELENE mission, covering a total of 14 months, from January 2008 until February 2009, were processed and the results were presented. Orbit determination using VLBI data showed that orbit consistency is greatly improved: without VLBI data, orbit prediction analysis resulted in orbit differences of several hundreds of metres, but including the VLBI data brought these differences down to a few tens of metres. Including these precise data also enabled extension of the arc lengths of Rstar and Vstar. The rms of the VLBI residuals was in general better than 1 cm. From previous analysis, the intrinsic noise level of the VLBI data has been estimated to be as low as a few mm, but orbit prediction analysis with different data weights showed that the smallest (and most consistent) orbit differences were obtained for a data weight of 1 cm for VLBI data, combined with Doppler data weighted at 1 mm/s and range data weighted at 2 m.

Using these results from orbit determination, and the full set of SELENE tracking data, the lunar gravity field was determined in a spherical harmonics expansion up to degree and order 100. Other data included were pre-SELENE tracking data from the Lunar Orbiters I–V, the Apollo 15 and 16 sub-satellites, Clementine, Lunar Prospector nominal mission data, and some SMART-1 data. Compared with the previous SELENE gravity field model named SGM100h (that used much of the same processing used in the work presented here, except for the VLBI data and accompanying longer arc lengths), the new model, named SGM100i, shows improved correlations with topography over the lunar far side, the area where also the largest gravity anomaly differences with

SGM100h were found. Orbit determination analysis also showed improved performance for the new model over previous 100 degrees and order models, indicating that the anomaly differences over the far side are an actual improvement. This, thus, shows the subtle influence of the VLBI data in the processing of SELENE data: through improved positioning of Rstar, the 4-way data were also affected positively. Overall, the strength of the VLBI data was demonstrated, including the benefits that can be obtained from including a precise tracking data type such as differential VLBI data. The new model can be downloaded through the following two websites: http://www.soac.selene.isas.jaxa.jp/archive/ and http://www.miz.nao.ac.jp/rise-pub/en.

Other future planetary missions might benefit from including VLBI data as well. There are some limitations, however, to the method as used in SELENE. For example, due to limitations on the usable bandwidth, the accuracy of the group delay to determine the ambiguity of the phase delay is not enough beyond lunar orbit, which means that SELENE's multi-frequency method cannot be used and different methods are needed for planetary orbiters. However, if the a priori delays are precise enough, for example from an orbit determined with Doppler data, or if a bias is estimated on the VLBI data, the ambiguities might be determined from this information, yielding a precise measurement (e.g. Border et al. 1992; Folkner et al. 1993). If that is not an option, delay-rates instead of delays might be used, although the question whether the ambiguities are needed for this is currently still under consideration. In terms of future lunar exploration, proposed tandem-satellite missions might benefit from same-beam differential VLBI, with the contribution of VLBI depending on whether its precision complements an already precise inter-satellite link.

The VLBI data were also expected to improve the estimates of the lower degrees, but the formal errors of these coefficients are only slightly smaller than those for SGM100h. It was shown that these degrees remain difficult to determine from current limited arc lengths. Coefficient differences between SGM100h and SGM100i are still proportionately large for the lower degrees, compared with the accompanying formal errors. On the one hand this shows that the lower degrees were affected by the VLBI data and the extension of the arc lengths of the sub-satellites, but on the other hand this discrepancy is also an indication of issues with calibration, which remains difficult for lunar gravity field models.

The lunar degree 2 potential Love number k_2 was also determined, and including the VLBI data resulted in a slightly higher value of 0.0255 ± 0.0016 versus 0.0240 ± 0.0015 for SGM100h. Correlations between k_2 and the $C_{2,2}$ coefficient were, however, found to be high, at -0.41, indicating perhaps a low separability between these parameters. Despite using longer arc lengths for Rstar and Vstar, this could be due to data quantities for these sub-satellites. As in previous analysis, Lunar Prospector data still contribute a lot to the determination of the lower degrees and k_2. Future analysis will thus focus on extending arc lengths for Lunar Prospector using SGM100i as a priori gravity field model, which might lead to further constraints on the lower degrees, Love number and lunar moments of inertia.

Acknowledgments We would like to express our appreciation to the engineers of NEC/Toshiba Space Systems Ltd. (NTS), Nippon Antenna Co. Ltd., and Nippi Corporation who developed the on-board instruments and the sub-satellites. We would also like to thank the entire staff of the SELENE project, especially the flight directors for both Rstar and Vstar who supervised the tracking of these two sub-satellites. We would especially like to thank all the colleagues at RISE Project, Mizusawa, who helped with the VLBI observations and data correlation. We thank Alex Konopliv (JPL) and two other anonymous reviewers for their comments that helped to improve this paper. VLBI tracking data files and the new model are available through the SELENE Data archive website at http://www.soac.selene.isas.jaxa.jp/archive/. The models are also available through the RISE Data archive website at http://www.miz.nao.ac.jp/rise-pub/en. All figures were drawn using the free software package GMT (Wessel and Smith 1991). Localised spherical harmonic analyses were performed using the freely available software archive SHTOOLS (available at http://www.ipgp.fr/~wieczor/SHTOOLS/SHTOOLS.html). This work was supported by Grant-in-Aid for Scientific Research (A) (No.20244073) from the Japan Society for the Promotion of Science. Finally, we like to mention that the gravity experiments of SELENE would not have been possible without the expertise of Fumio Fuke, an engineer of NTS, who sadly passed away 2 months after the launch of the mission.

References

Araki H, Tazawa S, Noda H, Ishihara Y, Goossens S, Sasaki S, Kawano N, Kamiya I, Otake H, Oberst J, Shum C (2009) Lunar global shape and polar topography derived from Kaguya-LALT laser altimetry. Science 323:897–900. doi:10.1126/science.1164146

Bills BG (1995) Discrepant estimates of moments of inertia of the Moon. J Geophys Res 100(E12):26297–26303

Border JS, Folkner WM, Kahn RD, Zukor KS (1992) Precise tracking of the Magellan and Pioneer Venus Orbiters by same-beam interferometry. Part I: data accuracy analysis. Tech. Rep. TDA Progress Report 42-110, Jet Propulsion Laboratory

Carranza E, Konopliv A, Ryne M (1999) Lunar prospector orbit determination uncertainties using the high resolution lunar gravity field models. In: Advances in the astronautical sciences. AAS/AIAA astrodynamics specialist conference, Girdwood, Alaska, vol 103, pp 381–400. AAS paper 99-325

Counselman CC III (1973) Very-long baseline interferometry techniques applied to problems of geodesy, geophysics, planetary science, astronomy, and general relativity. Proc IEEE 61(9):1225–1230

Counselman CC III, Hinteregger HF, Shapiro II (1972) Astronomical applications of differential interferometry. Science 178:607–608

Counselman CC III, Hinteregger HF, King RW, Shapiro II (1973) Precision selenodesy via differential interferometry. Science 181:772–774

Counselman CC III, Gourevitch SA, King RW, Pettengill GH, Prinn RG, Shapiro II, Miller RB, Smith JR, Ramos R, Liebrecht P (1979) Wind velocities on Venus: vector determination by radio interferometry. Science 203:805–806

Floberghagen R (2002) Lunar gravimetry, astrophysics and space science library, vol 273. Kluwer Academic Publishers, Dordrecht

Folkner WM, Border JS, Nandi S, Zukor KS (1993) Precise tracking of the Magellan and Pioneer Venus Orbiters by same-beam interferometry. Part II: Orbit determination analysis. Tech. Rep. TDA Progress Report 42-113. Jet Propulsion Laboratory

Folkner WM, Williams JG, Boggs DH (2009) The Planetary and Lunar Ephemeris DE 421. Tech. Rep. IPN Progress Report 42-178. Jet Propulsion Laboratory

Goossens S, Matsumoto K (2007) Lunar satellite orbit determination analysis and quality assessment from Lunar Prospector tracking data and SELENE simulations. Adv Space Res 40(1):43–50. doi:10.1016/j.asr.2006.12.008

Goossens S, Matsumoto K (2008) Lunar degree 2 potential Love number determination from satellite tracking data. Geophys Res Lett 35:L02204. doi:10.1029/2007GL031960

Hanada H, Iwata T, Namiki N, Kawano N, Asari K, Ishikawa T, Kikuchi F, Liu Q, Matsumoto K, Noda H, Tsuruta S, Goossens S, Iwadate K, Kameya O, Tamura Y, Hong X, Ping J, Aili Y, Ellingsen S, Schlüter W (2008) VLBI for better gravimetry in SELENE. Adv Space Res 42:341–346. doi:10.1016/j.asr.2007.11.003

Hanada H, Iwata T, Liu Q, Kikuchi F, Matsumoto K, Goossens S, Harada Y, Asari K, Ishikawa T, Ishihara Y, Noda H, Tsuruta S, Petrova N, Kawano N, Sasaki S, Sato K, Namiki N, Kono Y, Iwadate K, Kameya O, Shibata KM, Tamura Y, Kamata S, Yahagi Y, Masui W, Tanaka K, Maejima H, Hong X, Ping J, Shi X, Huang Q, Aili Y, Ellingsen S, Schlüter W (2010) Overview of differential VLBI observations of lunar orbiters in SELENE (Kaguya) for precise orbit determination and lunar gravity field study. Space Sci Rev 154:123–144. doi:10.1007/s11214-010-9656-9

Heki K, Matsumoto K, Floberghagen R (1999) Three-dimensional tracking of a lunar satellite with differential very-long baseline-interferometry. Adv Space Res 23(11):1821–1824

Kato M, Sasaki S, Tanaka K, Iijima Y, Takizawa Y (2008) The Japanese lunar mission SELENE: science goals and present status. Adv Space Res 42(2):294–300. doi:10.1016/j.asr.2007.03.049

Kaula WM (1966) Theory of Satellite Geodesy, applications of satellites to Geodesy. Blaisdell Publishing Company, Waltham

Kikuchi F, Liu Q, Matsumoto K, Hanada H, Kawano N (2008) Simulation analysis of differential phase delay estimation by same beam VLBI method. Earth Planets Space 60:391–406

Kikuchi F, Liu Q, Hanada H, Kawano N, Matsumoto K, Iwata T, Goossens S, Asari K, Ishihara Y, Tsuruta S, Ishikawa T, Noda H, Namiki N, Petrova N, Harada Y, Ping J, Sasaki S (2009) Pico-second accuracy VLBI of the two sub-satellites of SELENE (KAGUYA) using multi-frequency and same-beam methods. Radio Sci 44(RS2008). doi:10.1029/2008RS003997

King RW, Counselman CC III, Shapiro II (1976) Lunar dynamics and selenodesy: results from analysis of VLBI and laser data. J Geophys Res 81(35):6251–6256

Kobayashi H, Sasao T, Kawaguchi N, Manabe S, Omodaka T, Kameya O, Shibata KM, Miyaji T, Honma M, Tamura Y, Hirota ST, Kuji S, Horiai K, Sakai S, Sato K, Iwadate K, Kanya Y, Ujihara H, Jike T, Fujii T, Oyama T, Kurayama H, Suda H, Sakakibara S, Kamohara R, Kasuga T (2003) VERA project. In: Minh YC (ed) Astronomical Society of the Pacific Conference Series, vol 306, pp 48P+

Kono Y, Hanada H, Ping J, Koyama Y, Fukuzaki Y, Kawano N (2003) Precise positioning of spacecrafts by multi-frequency VLBI. Earth Planets Space 55:581–589

Konopliv AS, Yuan DN (1999) Lunar prospector 100th degree gravity model development. In: 30th Lunar and Planetary Science Conference. Abstract number 1067

Konopliv AS, Sjogren WL, Wimberly RN, Cook RA, Vijayaraghavan A (1993) A high resolution lunar gravity field and predicted orbit behavior. In: AAS/AIAA astrodynamics conference, Victoria, British Columbia, Canada, pp 1275–1294. AAS Paper 93-622

Konopliv AS, Binder AB, Hood LL, Kucinkas AB, Sjogren WL, Williams JG (1998) Improved gravity field of the Moon from lunar prospector. Science 281(5382):1476–1480

Konopliv AS, Asmar SW, Carranza E, Sjogren WL, Yuan DN (2001) Recent gravity models as a result of the Lunar Prospector Mission. Icarus 150:1–18

Lemoine FGR, Smith DE, Zuber MT, Neumann GA, Rowlands DD (1997) A 70th degree lunar gravity model (GLGM-2) from Clementine and other tracking data. J Geophys Res 102(E7):16,339–16,359

Liu Q, Kikuchi F, Matsumoto K, Asari K, Tsuruta S, Ping J, Hanada H, Kawano N (2007) Error analysis of same-beam differential VLBI technique using two selene satellites. Adv Space Res 40(1):51–57. doi:10.1016/j.asr.2007.02.044

Liu Q, Kikuchi F, Matsumoto K, Goossens S, Hanada H, Harada Y, Shi X, Huang Q, Ishikawa T, Tsuruta S, Asari K, Ishihara Y, Kawano N, Kamata S, Iwata T, Noda H, Namiki N, Sasaki S, Ellingsen S, Sato K, Shibata K, Tamura Y, Jike T, Iwadate K, Kameya O, Ping J, Xia B, An T, Fan Q, Hong X, Yang W, Zhang H, Aili Y, Reid B, Hankey W, McCallum J, Kronschnabl G, Schlüter W (2010a) Same-beam VLBI observations of SELENE for improving lunar gravity field model. Radio Sci 45(RS2004). doi:10.1029/2009RS004203

Liu Q, Matsumoto K, Iwata T, Namiki N, Noda H, Hanada H, Ishihara Y, Goossens S, Kikuchi F, Asari K, Tsuruta S, Ishikawa T, Sasaki S, Takano T (2010b) Effect of in-situ phase characteristics of antennas onboard flying spin satellites on Doppler measurements for lunar gravity field. IEEE Trans Aerospace Electron Syst (in press)

Luthcke SB, Marshall JA, Rowton SC, Rachlin KE, Cox CM, Williamson RG (1997) Enhanced radiative force modelling of the tracking and data relay satellites. J Astronaut Sci 45(3):349–370

Marshall JA, Luthcke SB (1994) Modeling radiation forces acting on TOPEX/Poseidon for precision orbit determination. J Spacecraft Rockets 31(1):99–105

Matsumoto K, Hanada H, Namiki N, Iwata T, Goossens S, Tsuruta S, Kawano N, Rowlands DD (2008) A simulation study for anticipated accuracy of lunar gravity field model by SELENE tracking data. Adv Space Res 42:331–336. doi:10.1016/j.asr.2007.03.066

Matsumoto K, Goossens S, Ishihara Y, Liu Q, Kikuchi F, Iwata T, Namiki N, Noda H, Hanada H, Kawano N, Lemoine FG, Rowlands DD (2010) An improved lunar gravity field model from SELENE and historical tracking data: revealing the farside gravity features. J Geophys Res 115(E06007). doi:10.1029/2009JE003499

Mazarico E, Lemoine FG, Han SC, Smith DE (2010) GLGM-3, a degree 150 lunar gravity model from the historical tracking data of NASA Moon orbiters. J Geophys Res 115(E05001). doi:10.1029/2009JE003472

Namiki N, Hanada H, Tsubokawa T, Kawano N, Ooe M, Heki K, Iwata T, Ogawa M, Takano TRSAT/VRAD/LALT Mission Groups (1999) Selenodetic experiments of SELENE: relay subsatellite, differential VLBI and laser altimeter. Adv Space Res 23(11):1817–1820

Namiki N, Iwata T, Matsumoto K, Hanada H, Noda H, Goossens S, Ogawa M, Kawano N, Asari K, Tsuruta S, Ishihara Y, Liu Q, Kikuchi F, Ishikawa T, Sasaki S, Aoshima C, Kurosawa K, Sugita S, Takano T (2009) Farside gravity field of the Moon from four-way Doppler measurements of SELENE (Kaguya). Science 323:900–905. doi:10.1126/science.1168029

Pavlis DE, Poulose S, McCarthy J (2006) GEODYN II system description, vols. 1–5. Contractor report, SGT Inc., Greenbelt, MD

Preston RA, Hildebrand CE, Purcell GH, Ellis J, Stelzried CT, Finley SG, Sagdeev RZ, Linkin VM, Kerzhanovich VV, Altunin VI,

Kogan LR, Kostenko VI, Matveenko LI, Pogrebenko SV, Strukov IA, Akim EL, Alexandrov YN, Armand NA, Bakitko RN, Vyshlov AS, Bogomolov AF, Gorchankov YN, Selivanov AS, Ivanov NM, Tichonov VF, Blamont JE, Boloh L, Laurans G, Boischot A, Biraud F, Ortega-Molina A, Rosolen C, Petit G (1986) Determination of Venus winds by ground-based radio tracking of the VEGA balloons. Science 231:1414–1416. doi:10.1126/science.231.4744.1414

Sagdeev RZ, Linkin VM, Blamont JE, Preston RA (1986) The VEGA Venus balloon experiment. Science 231:1407–1408

Salzberg IM (1973) Tracking the Apollo lunar rover with interferometry techniques. Proc IEEE 61(9):1233–1236

Seeber G (2003) Satellite geodesy: foundations, methods, and applications. Walter de Gruyter GmbH & Co., Berlin

Thornton CL, Border JS (2000) Radiometric tracking techniques for deep-space navigation. Monograph 1, deep-space communications and navigation series. Jet Propulsion Laboratory, JPL Publication 00-11

Ullman R (2002) SOLVE program, users guide. Contract nas5-31760, task 103, Raytheon STX corporation. Revised by J.J. McCarthy

Wessel P, Smith WHF (1991) Free software helps map and display data. EOS Trans AGU 72:441

Wieczorek MA, Simons FJ (2005) Localized spectral analysis on the sphere. Geophys J Int 162:655–675. doi:10.1111/j.1365-246X.2005.02687.x

Wieczorek MA, Joliff BL, Khan A, Pritchard ME, Weiss BP, Williams JG, Hood LL, Righter K, Neal CR, Shearer C, McCallum IS, Tompkins S, Hawke BR, Peterson C, Gillis JJ, Bussey B (2006) The constitution and structure of the lunar interior. Rev Mineral Geochem 60:221–364

Williams JG, Boggs DH (2008) Lunar core and mantle. What does LLR see? In: Proceedings of the 16th international workshop on laser ranging, Poznan, Poland, pp 101–121

Williams JG, Boggs DH, Yoder CF, Ratcliff JT, Dickey JO (2001) Lunar rotational dissipation in solid body and Molten core. J Geophys Res 106(E11):27933–27968

Williams JG, Boggs DH, Folkner WM (2008) DE421 lunar orbit, physical librations, and surface conditions. Technical report, Jet Propulsion Laboratory, JPL Memorandum IOM 335-JW, DB, WF-20080314-001

Williams JG, Boggs DH, Ratcliff JT (2010) Lunar fluid core moment. In: 41st Lunar and planetary science conference. Abstract 2336

Witasse O, Lebreton J, Bird MK, Dutta-Roy R, Folkner WM, Preston RA, Asmar SW, Gurvits LI, Pogrebenko SV, Avruch IM, Campbell RM, Bignall HE, Garrett MA, van Langevelde HJ, Parsley SM, Reynolds C, Szomoru A, Reynolds JE, Phillips CJ, Sault RJ, Tzioumis AK, Ghigo F, Langston G, Brisken W, Romney JD, Mujunen A, Ritakari J, Tingay SJ, Dodson RG, van't Klooster CGM, Blancquaert T, Coustenis A, Gendron E, Sicardy B, Hirtzig M, Luz D, Negrao A, Kostiuk T, Livengood TA, Hartung M, de Pater I, Ádámkovics M, Lorenz RD, Roe H, Schaller E, Brown M, Bouchez AH, Trujillo CA, Buratti BJ, Caillault L, Magin T, Bourdon A, Laux C (2006) Overview of the coordinated ground-based observations of Titan during the Huygens mission. J Geophys Res 111(E10). doi:10.1029/2005JE002640